Published in final edited form as:
Aging Cell. 2011 October ; 10(5): 807–823. doi:10.1111/j.1474-9726.2011.00721.x.

DLP1-Dependent Mitochondrial Fragmentation Mediates 1-methyl-4-phenylpyridinium Toxicity in Neurons: Implications for Parkinson's Disease

Xinglong Wang[1], **Bo Su**[1], **Wanhong Liu**[2], **Xiaohua He**[2], **Yuan Gao**[1], **Rudy J. Castellani**[3], **George Perry**[1,4], **Mark A. Smith**[1], and **Xiongwei Zhu**[1]

[1]Department of Pathology, Case Western Reserve University, Cleveland, Ohio USA

[2]School of Medicine, Wuhan University, Wuhan, Hubei, China

[3]Department of Pathology, University of Maryland, Baltimore, Maryland USA

[4]College of Sciences, University of Texas at San Antonio, San Antonio, Texas USA

SUMMARY

Selective degeneration of nigrostriatal dopaminergic neurons in Parkinson disease (PD) can be modeled by the administration of the neurotoxin 1-methyl-4-phenylpyridinium (MPP^+). Since abnormal mitochondrial dynamics are increasingly implicated in the pathogenesis of PD, in this study, we investigated the effect of MPP^+ on mitochondrial dynamics and assessed temporal and causal relationship with other toxic effects induced by MPP^+ in neuronal cells. In SH-SY5Y cells, MPP^+ causes a rapid increase in mitochondrial fragmentation followed by a second wave of increase in mitochondrial fragmentation, along with increased DLP1 expression and mitochondrial translocation. Genetic inactivation of DLP1 completely blocks MPP^+-induced mitochondrial fragmentation. Notably, this approach partially rescues MPP^+-induced decline in ATP levels and ATP/ADP ratio and increased $[Ca^{2+}]_i$ and almost completely prevents increased reactive oxygen species production, loss of mitochondrial membrane potential, enhanced autophagy and cell death, suggesting that mitochondria fragmentation is an upstream event that mediates MPP^+-induced toxicity. On the other hand, thiol antioxidant NAC or glutamate receptor antagonist D-AP5 also partially alleviate MPP^+-induced mitochondrial fragmentation, suggesting a vicious spiral of events contributes to MPP^+-induced toxicity. We further validated our findings in primary rat midbrain dopaminergic neurons that 0.5 μM MPP^+ induced mitochondrial fragmentation only in TH-positive dopaminergic neurons in a similar pattern to that in SH-SY5Y cells but had no effects on these mitochondrial parameters in TH-negative neurons. Overall, these findings suggest that DLP1-dependent mitochondrial fragmentation plays a crucial role in mediating MPP^+-induced mitochondria abnormalities and cellular dysfunction and may represent a novel therapeutic target for PD.

Keywords

MPP+; mitochondrial dynamics; Parkinson disease; DLP1/Drp1; mitochondrial fragmentation; neurotoxicity

Corresponding Author: Xiongwei Zhu, Ph.D. Department of Pathology Case Western Reserve University 2103 Cornell Road Cleveland, Ohio 44106 USA Tel: 216-368-5903 Fax: 216-368-8964 xiongwei.zhu@case.edu.

AUTHOR CONTRIBUTIONS: XW and XZ designed experiments, interpreted data and wrote the manuscript. XW performed most experiments and obtained most results. BS and YG performed some experiments. RJC, GP and MAS helped with data interpretation.

INTRODUCTION

Parkinson's disease (PD) is a progressive neurodegenerative movement disorder characterized by loss of nigrostriatal dopaminergic neurons. Familial genetically-based PD accounts for less than 10% of all cases, with the majority of PD cases being sporadic. While the etiology of sporadic PD has not been completely elucidated, there is growing concerns that environmental factors, such as exposure to neurotoxins increase risk to develop PD[1]. In this regard, 1-methyl-4-phenyl-1,2,3,6-tetrahydropyridine (MPTP), via its active metabolite 1-methyl-4-phenylpyridinium ion (MPP^+), may be a contributing issue in the etiopathogenesis of the disease. MPTP causes parkinsonism in humans and non-human primates by decreasing dopamine levels and tyrosine hydroxylase activity, impairing dopamine uptake, and eliciting dopaminergic neuronal loss. As such, both MPTP and MPP^+ have been extensively used in a variety of *in vivo* mammalian species and *in vitro* paradigms as experimental models of PD, respectively[2]. Given the parallels with PD, further understanding the mechanisms by which MPTP/MPP^+ lead to dopaminergic neuronal death could provide insights into therapeutic targets for PD.

Although the molecular events leading to the loss of dopaminergic neurons in PD remain elusive, there is compelling evidence that mitochondrial dysfunction represent a critical event[3]. In sporadic PD, consistent and significant deficits in both subunits and activity of mitochondrial respiratory chain complex 1 are found in the substantia nigra and blood platelets of PD patients as well as in cytoplasmic hybrid cell line (cybrids)[4–6]. MPP^+ is generally thought to induce cell death by targeting mitochondria[7], specifically blocking NADH-dehydrogenase-linked oxidation and leading to a loss in ATP and increased production of reactive oxygen species (ROS). MPP^+ also elicits increased mitochondrial degradation through enhanced autophagy[8].

Mitochondria are dynamic organelles that constantly divide by a fission process and also fuse with each other—processes regulated by machinery involving large dynamin-related GTPases that exert opposing effects; e.g., dynamin-like protein 1 (DLP1) for fission, and optic atrophy 1 (OPA1) for fusion[9–11]. Recent evidence suggests that mitochondrial dynamics are critical for the maintenance of a variety of mitochondrial functions including ATP production, calcium homeostasis, ROS production and the regulation of apoptosis[12]. Given this, it is perhaps not surprising that abnormal mitochondrial dynamics are implicated in various neurodegenerative diseases including PD[13–16]. However, to date, the impact of MPP^+ on mitochondrial dynamics remains unknown. To address this, in this study, we determined whether MPP^+ induced abnormal changes in mitochondrial dynamics and determined the temporal and causal relationship between changes in mitochondrial dynamics and MPP^+-induced mitochondrial abnormalities and neuronal death.

RESULTS

MPP^+ Induced Dose-Dependent Mitochondrial Fragmentation in SH-SY5Y Cells

To investigate the effect of MPP^+ on mitochondrial morphology, SH-SY5Y cells were transfected with mito-DsRed2, a red fluorescent protein that specifically targets the mitochondrial matrix. Two days after transfection, cells were treated with a range of concentrations (0.1 μM to 10 mM) of MPP^+ for 24 h. Cells were fixed, labeled with a specific antibody against tubulin, and immunolocalization visualized by laser confocal microscopy (Figure 1A). As reported previously[17], mitochondria demonstrate a tubular and filamentous morphology in the majority (>95%) of control SH-SY5Y cells. On the other hand, MPP^+ treatment at concentrations greater than 10 μM induced a significant dose-dependent increase in the percentage of cells with fragmented mitochondria as evidenced by the appearance of small round structures (Figure 1 B). No changes in cytoskeleton structure

were noted as evidenced by the near identical immunostaining pattern of tubulin between MPP^+-treated and untreated cells (Figure 1A). Of note, MPP^+-induced mitochondrial fission is unlikely due to MPP^+-induced cell death since MPP^+-induced cell death only occurred at concentrations greater than 1 mM (Figure 1C). To delineate the temporal relationship between MPP^+-induced mitochondrial fission and other mitochondrial deficits and cell death, in the following experiments, we chose to use 2.5 mM MPP^+, a concentration that induced a modest degree of cell death (i.e., 17.8±3.1% and 42.9±4.5% cell death at 24 and 48 h respectively).

MPP^+ Induced A Time-Dependent Biphasic Increase in Mitochondrial Fragmentation in SH-SY5Y Cells

We next performed a time course study to determine the effect of MPP^+ on mitochondrial morphology (Figure 1D–F). Two days after transfection with mito-DsRed2, SH-SY5Y cells were treated with 2.5mM MPP^+ and fixed at different time points. Typical filamentous and tubular mitochondria were noted in the majority (>95%) of non-treated cells during the course of the experiments. In contrast, MPP^+ exposure led to rapid mitochondrial fragmentation as evidenced by the appearance of small round mitochondria in 23.9±2.7% of cells within 1 h (Figure 1D). Interestingly, while the percentage of cells with fragmented mitochondria gradually increased after 1 h of treatment, there was a second wave of increase in the percentage of cells with fragmented mitochondria after 4 h of treatment which led to approximately 65.4±2.2% of cells demonstrating fragmented mitochondria at 12 h and thereafter.

To track the effects of MPP^+ on mitochondrial morphology in single cells in real time, SH-SY5Y cells were seeded on glass-bottomed dishes and transfected with mito-DsRed2. Two days after transfection, cells were placed in a well-equipped live imaging station with controlled CO_2 content, humidity and temperature. Live cell imaging by fluorescence time-lapse microscopy was performed (Figure 1E). Positively-transfected cells with normal cell shape were chosen and imaged at one frame per 5 min for 24 h. No phototoxicity was noted during recording (not shown). Consistent with our time course study on fixed cells (Figure 1D), we observed a pronounced fragmentation of single tubular mitochondria into small round organelles as early as 1 h (Figure 1E). Interestingly, by following more than 100 cells treated with MPP^+, we also observed a biphasic pattern in mitochondrial length: aspect ratio (ratio of length/width as an index of mitochondria morphology), which significantly decreased from 2.91±0.04 to 2.72±0.04 during the first hour (Figure 1F). This initial decrease persisted for several hours and was followed by a second wave of decrease that resulted in mitochondria with an average aspect ratio of 1.93±0.03 at 16 h and thereafter.

MPP^+ Induced Changes in DLP1 Expression and Mitochondria Recruitment

In mammalian cells, DLP1 plays a critical role in mitochondrial fission[10]. To determine whether DLP1 is involved in MPP^+-induced mitochondrial fragmentation in SH-SY5Y cells, we first measured the total expression level of DLP1 in SH-SY5Y cells treated with 2.5 mM MPP^+ up to 48 h by western blot. Consistent with the fragmentation phenotype, DLP1 levels began to increase as early as 30 min after MPP^+ treatment, and continued to increase until 8 h after treatment and decreased gradually thereafter. DLP1 levels diminished significantly 48 h after treatment (Figure 2A and B).

The majority of DLP1 resides in the cytoplasm, and is recruited to punctate spots on the mitochondrial surface during fission[18]. Therefore, we also determined whether there was increase in mitochondrial recruitment of DLP1 during MPP^+ treatment by measuring levels of mitochondrial DLP1 (mito-DLP1) in MPP^+-treated SH-SY5Y cells in two ways. First, we performed immunofluorescent analysis of the levels of DLP1 colocalizing with

mitochondria in SH-SY5Y cells. Two days after transfection with mito-DsRed2, SHSY5Y cells were treated with 2.5 mM MPP^+ for various periods of time, and then fixed, and stained by a specific antibody against DLP1. Compared with control cells, in which DLP1 only sparsely colocalized with mitochondria, MPP^+ significantly increased DLP1 colocalziation with mitochondria (Figure 2C). Quantification analysis revealed that the levels of mito-DLP1 (intensity of green signal that co-localizes with red signal/red signal) was rapidly increased and peaked within 1 h of treatment of MPP^+, began to plateau at 2 h and was maintained thereafter until 48 h of treatment (Figure 2D). Second, we conducted subcellular fractionation experiments and the levels of mito-DLP1 were determined by immunoblot using anti-DLP1 antibody in mitochondrial fractions (Figure 2E and F). As internal controls, levels of mitochondrial protein COX-IV were determined and the purity of the mitochondrial fraction preparation was confirmed by a lack of GAPDH or Calnexin immunoreactivity (Figure 2E). Consistent with the immunofluoresent analysis, the levels of mito-DLP1 rapidly increased, peaked within 1 h of treatment of MPP^+, began to plateau at 2 h and maintained thereafter until 24 h and then increased again at 48 h of treatment (Figure 2F).

MPP^+-Induced Mitochondrial Fission Was Completely Abolished by Silencing of DLP1

To causally corroborate the role of DLP1 in MPP^+–induced mitochondrial fragmentation, SH-SY5Y cells were transiently transfected with either GFP-tagged DLP1 RNAi constructs or GFP-tagged dominant-negative mutant DLP1(K38A) together with mito-DsRed2. Immunoblots of cell lysates from cells transiently transfected with DLP1 RNAi constructs (transfection efficiency is around 80%) confirmed that DLP1 protein levels were reduced to 40% of control levels whereas no changes in DLP1 levels were noted in cells transfected with control RNAi constructs (Figure 3C). 2 days after transfection, cells were treated with 2.5 mM MPP^+ for various periods of time, fixed, stained and imaged. Not surprisingly, in contrast to the short tubular or filamentous mitochondrial morphology of control cells, both DLP1 knockdown or overexpression of dominant negative DLP1(K38A) mutant caused mitochondrial elongation as indicated by an elongated mitochondrial tubular network. Quantification revealed that both DLP1 knockdown or overexpression of DLP1(K38A) almost completely abolished MPP^+–induced mitochondrial fragmentation at 24 h (Figure 3A and B). In fact, following treatment of 2.5 mM MPP^+, cells lacking DLP1 or with DLP1(K38A) maintained an elongated tubular mitochondrial network throughout the 48 h incubation period (Figure 3D).

MPP^+ Caused Decreases in ATP levels Concurrent with Enhanced Mitochondrial Fragmentation

Since MPP^+ is an inhibitor of complex I and blocks respiration, we determined the effect of MPP^+ on intracellular ATP concentrations and ATP/ADP ratio as functional parameters of mitochondrial respiratory chain. SH-SY5Y cells were exposed to 2.5 mM MPP^+ and ATP levels and ATP/ADP ratio were measured after various incubation times. Treated cells demonstrated a rapid decrease in ATP (25.3%) within 1 h which persisted for 2–3 h and was followed by a second wave of decrease with a maximal drop of 44.8% at 12 h which was maintained until 24 h (Figure 4B). A similar rapid decrease in ATP/ADP ratio occurred within 1 hr, followed by a more gradual decrease until 12 hr and a plateau until 24 h (Figure 4C).

To explore the relationship between MPP^+-induced bioenergetic changes and mitochondrial fragmentation, we established three independent clones of SH-SY5Y cells stably transfected with GFP-tagged DLP1 RNAi constructs (DLP1 RNAi cells). DLP1 expression was decreased by 87% in DLP1 RNAi cells and expression of RNAi resistant DLP1 restored DLP1 levels in these cell lines as confirmed by western blot (Figure 4A). Similar to the

transient transfection experiments, mitochondrial fragmentation was completely abolished in these cell lines despite treatment with 2.5 mM MPP^+ for up to 48 h (data not shown). We measured intracellular ATP levels and ATP/ADP ratio in these DLP1 RNAi cells and found that basal levels of ATP and ATP/ADP ratio were similar in non-treated DLP1 RNAi cells compared to control cells (not shown). Interestingly, although DLP1 knockdown did not completely prevent the MPP^+-induced initial decline in ATP, it did significantly attenuate such decline to 12.6% at 1 h followed by a much more gradual loss with the maximal decline of 16.9% at 24 h (Figure 4B). Similarly, although DLP1 knockdown did not completely prevent the initial decline in ATP/ADP ratio, it did prevent the subsequent gradual decline (Figure 4C). In contrast, in cells transfected with negative-control RNAi (negative control cells), MPP^+-induced decline in ATP and ATP/ADP ratio were indistinguishable from MPP^+-treated non-transfected controls (control cells) (Figure 4B and C).

As ATP reduction could be due to impaired glycolysis or impaired mitochondrial respiration, we performed additional experiments with 2-deoxyglucose (2-DG), an inhibitor of glycolysis, or antimycin A, a complex III inhibitor to assess the contribution of glycolysis or mitochondrial respiration. In SH-SY5Y or DLP1 knockdown cells, 5 μM antimycin A caused ATP decrease by 77% within 2 hours followed by a slight and more gradual decrease until 24 h (Figure 4D) while 2-DG resulted in a mild decrease of 21% in ATP levels within 2 h followed by a slight and more gradual decrease until 24 h (Figure 4E). Based on these observations, SH-SY5Y cells were first pre-incubated with 5 μM antimycin A or 1 mM2-DG for 2 hr to have ATP decline stabilized, and then treated with 2.5 mM MPP^+ for various period of time. MPP^+ treatment of SH-SY5Y cells pre-incubated with antimycin A did not result in further reduction of ATP, compared with cells treated with antimycin A only (Figure 4D). On the contrary, MPP^+ treatment of cells pre-incubated with 2-DG caused a rapid decrease in ATP levels within 1 hour followed by significant but more gradual decline until 24 hr (Figure 4E). Interestingly, in 2-DG pretreated DLP1 knockdown cells, although MPP^+ still induced a rapid decrease in ATP levels within 1 hr, the second phase of more gradual ATP decline was blocked (Figure 4E). Overall, these data suggest that 2-DG pretreatment did not affect MPP-induced ATP decline pattern (neither the first wave nor the second wave). Therefore, it is unlikely that impaired glycolysis contributes to MPP^+-induced ATP decline. Antimycin pretreatment abolishes both waves of MPP-induced ATP decline. However, since antimycin is so potent in ATP depletion, the possibility of floor effect that mask any changes that may be induced by MPP^+ treatment could not be ruled out. Nevertheless, given that MPP^+ was shown to be a specific inhibitor of complex I, we concluded that MPP^+ likely reduces ATP level primarily through mitochondrial respiration inhibition but not through glycolysis inhibition.

MPP^+-Induced Mitochondrial Fragmentation and ROS Production

Mitochondria are the primary source for endogenous ROS and significant increases in ROS levels could be detected in SH-SY5Y cells after 1 h treatment with 2.5 mM MPP^+ (Figure 5A). Interestingly, this initial increase persisted and was followed by a second wave of increase in ROS levels after 12 h of 2.5 mM MPP^+ treatment. There was a slight decrease of ROS at 48 h of treatment, probably due to loss of cell numbers at this time.

To explore the relationship between MPP^+-induced mitochondrial fragmentation and ROS production, we also measured ROS levels in stable DLP1 RNAi cells treated with 2.5mM MPP^+ for various period of time. Basal level of ROS were similar in non-treated DLP1 RNAi cells compared to control cells. Interestingly, MPP^+-induced ROS production was completely prevented in DLP1 RNAi cells up to 24 h. A slight but significant increased in ROS production in DLP1 RNAi cells was detected only after 48 h treatment with MPP^+

(Figure. 5B). These findings indicate that prevention of MPP^+-induced fragmentation prevents ROS production.

To further explore whether increased ROS production contributes to MPP^+-induced mitochondrial fragmentation, we pretreated SH-SY5Y cells with the thiol antioxidant N-acetylcysteine (NAC), which almost completely prevented MPP^+-induced ROS production (Figure 5B). No fragmentation was observed in SH-SY5Y cells treated with NAC alone for up to 48 h. We also studied the effect of NAC on MPP^+ -induced mitochondria fragmentation in cells fixed after treatment (Figure 5C). Consistent with our prior experiments, 87.6±1.3% of cells demonstrated fragmented mitochondria after 48 h treatment with 2.5 mM MPP^+, which was significantly reduced to 62.3±2.1% following NAC pretreatment. These data suggest that oxidative stress partially contributes to MPP^+-induced mitochondrial fragmentation (Figure 5C). We next determined the effect of MPP^+ on mitochondrial morphology in single cells in real time and found that NAC had no effect on the initial decline in mitochondria aspect ratio induced by MPP^+ within the first hour, but attenuated the second wave of decline in mitochondria aspect ratio to 2.03±0.033 at 24 h, compared with 1.81±0.029 in cells treated with MPP^+ alone (Figure 5D).

MPP^+-induced mitochondrial fragmentation and decreased mitochondrial membrane potential

Mitochondrial membrane potential (MMP) is a very important marker of the function of mitochondria and, here, we measured MMP using the fluorescence dye TMRM in SHSY5Y cells treated with 2.5mM MPP^+ for various periods of time (Figure 6A). Because changes in plasma membrane potential (PMP) could affect MMP measurement by TMRM, we also measured PMP by DiBAC4(5) during the course of MPP^+ treatment (Figure 6B). While MPP^+ treatment had no effect on PMP, it induced a rapid decrease in MMP within the first hour followed by a more gradual decline during the entire incubation period.

To explore the relationship between MPP^+-induced mitochondrial fragmentation and MMP decline, we also measured the PMP and MMP in stable DLP1 RNAi cells during the course of MPP^+ treatment (Figure 6A and B). Basal MMP was significantly increased in non-treated DLP1 RNAi cells compared to control cells (Figure. 6A). Importantly, MPP^+-treated DLP1 RNAi cells demonstrated no changes in MMP for 16 h and only a slight, but significant, decline in MMP was detected after 24 h of treatment (Figure 6A). No changes in PMP were noted in either negative control or DLP1 RNAi cells at basal level or during MPP^+ treatment (Figure 6B).

MPP^+-induced mitochondrial fragmentation was prerequisite for MPP^+-induced Autophagy/mitophagy

Since previous studies demonstrated that MPP^+ significantly increased autophagy in SHSY5Y cells[8], we explored the relationship between MPP^+-induced mitochondrial fragmentation and mitophagy in SH-SY5Y cells. The conversion of the cellular protein LC3 to LC3-II, which can bind to autophagic membranes, is an early hallmark of autophagy activation[19]. Levels of LC3 were measured by immunoblot in SH-SY5Y cells treated with 2.5mM MPP^+ for various periods of time (Figure 7A). Two bands of LC3 were noted, with the upper 18-kDa band corresponding to unmodified LC3-I and the lower band corresponding to LC3-II[19]. As expected, the level of LC3-II and the ratio of LC3-II/ LC3-I increased significantly in SH-SY5Y cells after 48 h treatment with 2.5 mM MPP (Figure 7A). To rule out the possibility that increased LC3-II was caused by deficits in LC3-II degradation due to impaired lysosmal turnover, we measured LC3 levels in the presence of 10 μg/ml E64 and pepstatin A, lysosomal protease inhibitors, which, as expected, led to increased levels of LC3II which were not further increased by 48 h (Figure 7B). More

importantly, the fact that E64/pepstatin A treatment markedly increased LC3-II levels in MPP^+-treated cells (Figure 7B, lane 3) compared to MPP^+ treatment alone (Figure 7B, lane 2), suggested that LC3-II degradation is intact after 48 h treatment of MPP^+. Collectively, these data confirmed an induction of autophagy in SHSY5Y cells by MPP^+ (Figure 7A, B). However, since there was no significant increase in LC3-II levels or in the ratio of LC3-II/LC3-I during the first 24 h treatment of 2.5 mM MPP^+, MPP^+-induced autophagy is a relatively late event.

To directly visualize autophagosome (APs) formation, we transiently transfected SHSY5Y cells with GFP-LC3 together with mito-DsRed2 constructs. Two days after transfection, cells were treated with 2.5 mM MPP^+ and imaged at different time points. To quantify differences between control and MPP^+-treated cells, we defined GFP-LC3 dots with a size larger than 0.3 μm as APs and GFP-LC3 (>0.3 μm) co-localizing with mitochondria as mitochondria containing APs as previously described[20]. Consistent with the LC-3 immunoblot study, a significant increase in the formation of APs or mitochondria containing APs in SH-SY5Y cells were noted only after 48 h of MPP^+ treatment, but not during the first 24 h (Figure 7C and D). We also assessed the effect of MPP^+ on autophagy and mitophagy by directly staining cells with a specific antibody against LC3 as previously described[21] after cells were fixed after various period of 2.5 mM MPP^+ treatment. Consistent with experiments using GFP-LC3, a significant increase in the formation of APs or mitochondria containing APs in SH-SY5Y cells were noted only after 48 h of MPP^+ treatment (Figure 7E and F). These imaging data confirm that MPP^+-induced autophagy is a relatively late event.

Since MPP^+-induced mitochondrial fragmentation occurs much earlier than autophagosome formation, we next asked whether MPP^+-induced mitochondrial fragmentation is required for MPP^+-induced increases in autophagy and mitophagy. SHSY5Y cells were transiently co-transfected with GFP-tagged DLP1 RNAi and mito-DsRed2 constructs and, 2 days after transfection, cells were treated with 2.5 mM MPP for 48 h and the number of APs or mitochondria-containing APs determined by image analysis. As expected, mitochondria demonstrated a tubular morphology in cells positively transfected by GFP-tagged DLP1 RNAi even in the presence of MPP^+ for 48 h (Figure 7G). Importantly, no increase in the number of APs or mitochondria-containing APs was found in these cells (Figure 7H). This finding was in contrast to the vector-control cells exposed to MPP^+ which demonstrated highly fragmented mitochondria along with increased number of APs or mitochondria-containing APs (Figure 7G and H). These findings suggest that DLP1 knockdown effectively blocks mitochondrial autophagy and this was further confirmed by immunoblot analysis demonstrating that LC3-II levels and the ratio of LC3-II/LC3-I was significantly reduced in DLP1 RNAi cells compared to negative control cells exposed to 2.5mM MPP^+ for 48 h (Figure 7I).

Activation of NMDA Receptor Activity Contributes to MPP^+-Induced Mitochondrial Fragmentation

Given that perturbations of intracellular Ca^{2+} ($[Ca^{2+}]_i$) homeostasis have been implicated in MPP^+-induced neuronal toxicity[22], we also explored the relationship between MPP^+-induced changes in $[Ca^{2+}]_i$ and mitochondrial fragmentation. We monitored $[Ca^{2+}]_i$ in living cells using Case12, a pH-stable circularly permuted fluorescent protein-based Ca^{2+} sensor sensitive to changes of calcium concentration in a physiological range from a hundred nanomoles to micromoles with a high signal-to-noise ratio. SH-SY5Y cells, seeded on glass-bottomed dishes, were transfected with Case12 plasmid. Two days after transfection, cells were imaged at one frame per 5 min for 24 h by fluorescence time-lapse microscopy. No phototoxicity was noted during the recording (not shown). Ca^{2+}-dependent Case12 fluorescence increased with a mean value of around 10% above baseline during the first 1 h

treatment with 2.5 mM MPP^+ (Figure 8C). This initial increase persisted for several hours and was followed by another wave of increase in $[Ca^{2+}]_i$ around 6–8 h after treatment. Because the green signal of GFP-tagged DLP1 RNAi interferes with the Case12 fluorescence signal, we established three stable SH-SY5Y cell lines overexpressing dominant-negative mutant DLP1 (i.e., DLP1 K38A) in which MPP^+-induced mitochondrial fragmentation was completely blocked (not shown). No changes in basal $[Ca^{2+}]_i$ levels were noted in these cell lines and while DLP1 K38A overexpression had no effect on the initial rapid increase in $[Ca^{2+}]_i$, it completely prevented the secondary increase of $[Ca^{2+}]_i$ (Figure 8E).

Activation of NMDA receptors can also contribute to MPP^+-induced excitotoxicity and perturbations in intracellular Ca^{2+} homeostasis[23]. We found that a NMDA receptor antagonist, D-AP5, had no effect on MPP-induced initial Ca^{2+} influx within the first several hours, but almost completely blocked the second wave of $[Ca^{2+}]_i$ increase (Figure 8D). To determine whether calcium influx has any effects on mitochondrial morphology, we examined the effect of D-AP5 on MPP^+-induced mitochondria fragmentation in cells fixed after 48 h treatment (Figure 8F). No fragmentation was observed in SH-SY5Y cells treated with D-AP5 only, however, consistent with prior experiments, approximately 90.3±1.7 % of cells demonstrated fragmented mitochondria after 48 h treatment with 2.5 mM MPP^+ which, following D-AP5 pretreatment, significantly reduced to 68.1±2.0% suggesting that NMDA receptor activation and perturbation of $[Ca^{2+}]_i$ homeostasis partially contributes to MPP^+-induced mitochondrial fragmentation (Figure 8F). We also investigated the effect of NMDA receptor activation on the MPP^+ induced biphasic increases in ROS (Figure 8G). Cells treated with D-AP5 alone did not cause any significant changes in ROS and while D-AP5 had no effect on the MPP^+-induced initial rapid ROS increase within 1 h, it completely blocked the second wave of ROS increase (Figure 8G), suggesting that NMDA receptor activation contributes to the second wave of ROS production.

MPP^+-Induced Mitochondrial Fragmentation Preceded and Was Prerequisite for Cell Death

Since MPP^+ can induce neuronal death, we investigated the temporal sequence between cell death and mitochondrial fragmentation induced by MPP^+ in SH-SY5Y cells. Cell viability after treatment of 2.5mM MPP^+ for various periods of time was determined by MTT and LDH release assays. Both assays revealed significant cell death in less than 20% cells after 24 h of treatment, increasing to approximately 40% and 90% at 48 h and 72 h, respectively (Figure 9A). These findings were supported by biochemical analysis of cleaved caspase-3 in SH-SY5Y cells treated with 2.5mM MPP^+. Increased levels of cleaved caspase 3 were first detected at 24 h and further increased at 48 h of MPP^+ treatment (Figure 9B). These data suggest that cell death occurs relatively late compared to mitochondrial fragmentation, supporting the notion that MPP^+-induced mitochondrial fragmentation is not simply a consequence of cell death. Consistent with this, treatment of cells with a pan-caspase inhibitor (e.g., Z-VAD-FMK) had no effect on mitochondrial fragmentation induced by MPP treatment (not shown). To determine a causal relationship, we further determined cell death in stable DLP1 RNAi cells exposed to 2.5 mM MPP^+. There were no changes in basal level of cell death in DLP1 RNAi or negative-control cell lines compared to non-transfected control cells. Supporting a causal role, no significant cell death was detected up to 48 h and only slight increases in cell death were detected in DLP1 RNAi cells at 72 h of 2.5mM MPP^+ treatment, in striking contrast to the 90% cell death in control cell lines. Overall, these data indicate that inhibition of mitochondrial fragmentation almost completely prevents MPP^+-induced cell death (Figure 9 C).

MPP^+ Induced Mitochondrial Fragmentation and Abnormal Distribution in Primary Rat Midbrain TH-Positive Dopaminergic Neurons

To determine whether MPP^+ exerts similar effects on mitochondria in differentiated primary dopaminergic neuronal cells, primary rat E18 midbrain neurons (DIV=6) were treated with 0.5 μM or 5 μM MPP^+. 24 hours after MPP^+ treatment, cells were fixed and stained. Interestingly, double-label immunofluoresence for tyrosine hydroxylase (TH) and COX-IV (marker of mitochondria) revealed that although 5 μM MPP^+ caused mitochondrial fragmentation in both TH-positive and TH-negative neurons (Figure 10B), 0.5 μM MPP^+ only elicited the appearance of small round mitochondria in both soma and neurites in TH-positive neurons, indicative of mitochondrial fragmentation, whereas 0.5 μM MPP^+-treated TH-negative neurons retained a tubular and filamentous morphology similar to non-treated control cultures (Figure 10A and B). Because 0.5 μM MPP^+ induced specific changes in mitochondrial morphology in TH-positive dopaminergic neurons, we used this concentration in subsequent time course studies. Because of the high density of mitochondria in the soma and proximal segment of axon, we focused on mitochondria in the distal segments of axons and axonal branches where mitochondria are separated from each other and easier to study in time course studies of mitochondrial length in primary midbrain dopaminergic neurons fixed at different time points after 0.5 μM MPP^+ treatment. Similar to SH-SY5Y cells, MPP^+ treatment caused a rapid mitochondrial fragmentation as early as 1 hour and a biphasic decrease in mitochondrial length in neuronal processes (Figure 10C): mitochondrial length rapidly decreased from 1.60 ± 0.06 μm in non-treated cells to 1.13 ± 0.04 μm within 4 h of MPP^+ treatment, persisted for around 8 h, followed by a further decrease to 0.62 ± 0.03 μm after 24 h of treatment. Despite an initial increased number of mitochondria in the neurite due to enhanced fission, the neurite mitochondria index (total mitochondrial length/neurite length in neuronal process 400 μm in length beginning from the cell body), a marker of mitochondrial coverage in neurites, decreased significantly from 0.22 ± 0.004/μm in control neurons to 0.19 ± 0.005/μm after 4 h of treatment, reaching a plateau at around 8 h and then further decreasing (Figure 10D).

DISCUSSION

In this study, we found that MPP^+ induces a DLP1-dependent biphasic increase in mitochondrial fragmentation in both SH-SY5Y neuroblastoma cells and primary rat dopaminergic midbrain neurons. As a specific inhibitor for complex I, MPP^+ induces a very rapid decrease in ATP and ATP/ADP ratio within 1 hr followed by a second wave of decrease after several hours and we found that MPP^+-induced mitochondrial fragmentation is also a temporally early event that occurs at a similar biphasic pattern. While it remains to be determined whether and how MPP^+-induced changes in bioenergetic function causes mitochondrial fragmentation, we demonstrated that excessive mitochondrial fragmentation exacerbates MPP^+-induced bioenergetic impairments and mediates the toxic effects of MPP^+ on mitochondrial membrane potential, calcium handling, ROS generation and mitophagy as well as eventual cell death. Indeed, attenuation of mitochondrial fragmentation by DLP1 knockdown reduces these downstream events induced by MPP^+. Given this, prevention of mitochondrial fragmentation is not only an attractive target to prevent MPP^+-induced deficits but may also have significant relevance to the treatment of PD. Mechanistically, we also show that increases in ROS and elevations in intracellular calcium contribute to MPP^+-induced mitochondrial fragmentation, suggesting the presence of a complex crosstalk between mitochondrial fragmentation, ROS production and calcium disturbances. To our knowledge, this is the first detailed study investigating the effect of MPP^+ on mitochondrial dynamics and its temporal and causal relationship with other toxic effects induced by MPP^+.

MPP^+ induces rapid mitochondrial fragmentation within 1 h of treatment and, while mitochondrial fragmentation can occur during cell death, MPP^+-induced mitochondrial fragmentation is unlikely an epiphenomenon due to neuronal death since at concentrations of MPP^+ that do not induce any cell death (i.e., 10–500 μM), a significant percentage of SH-SY5Y cells demonstrate increased mitochondrial fragmentation. Moreover, even at higher concentrations of MPP^+, significant cell death occurs only at very late time points (i.e., 48 or 72 h), much later than MPP^+-induced mitochondrial fragmentation. Consistent with this notion, preventing mitochondrial fragmentation completely blocks MPP^+-induced cell death whereas a pan-caspase inhibitor that operates upstream has no effects on MPP^+-induced fragmentation. Therefore, MPP^+-induced mitochondrial fragmentation not only precedes but is also a prerequisite for MPP^{+-}induced cell death.

Detailed time-lapse studies indicate that 2.5 mM MPP^+ induces a biphasic increase in the percentage of cells containing fragmented mitochondria with a very rapid initial increase within 1 h followed by a second wave of increase around 4 h after MPP^+ treatment. A similar biphasic decrease in mitochondrial length in single cells, as evidenced by decreased aspect ratio, was also observed in individual cells with fragmented mitochondria. At this time, it remains to be determined what directly causes mitochondrial fragmentation. Bioenergetic status and NAD^+ levels affect mitochondrial dynamics[24, 25] and it is possible that MPP^+-induced initial ATP reduction and/or changed NADH/NAD^+ ratio due to inhibition of complex I contributes to the early mitochondrial fragmentation. Nevertheless, other factors independent of complex-I function may also contribute[26]. Notably, MPP^+-induced mitochondrial fragmentation is accompanied by a rapid increase in mitochondrial recruitment of DLP1 and a more prolonged increase in total levels of DLP1, suggesting the involvement of DLP1. Supporting this, DLP1 knockdown or overexpression of dominant negative DLP1 could almost completely block MPP^+-induced mitochondrial fragmentation in SH-SY5Y cells, confirming the critical role of DLP1 in MPP^+-induced mitochondrial fragmentation. At this time, it is not clear how MPP^+ leads to increased DLP1 expression. Since the ubiquitin-proteasome system plays a critical role in DLP1degradation [27], it is possible that MPP^+-induced dysfunction of proteasomal activities contributes to increased DLP1 levels[28–30]. Nevertheless, despite the relative stable levels of mitochondrial DLP1 throughout 48 h treatment, total levels of DLP1 decreased at 48 h, which could be due to cleavage by activated caspases[31].

Consistent with previous studies, we found that MPP^+ induces a decline in intracellular ATP levels and ATP/ADP ratio[7]. In fact, our detailed time course studies revealed that MPP^+ induces ATP decline also in a biphasic manner: an immediate drop in ATP levels within 1 h followed by a second wave of decline around 4 h after MPP^+ treatment. A similar rapid drop in ATP/ADP ratio followed by more gradual but significant decline in ATP/ADP ratio was also noted. Interestingly, these two waves are temporally coincident with the two waves of mitochondrial fragmentation induced by MPP^+ treatment, suggesting a potential cause-effect relationship between mitochondrial fragmentation and bioenergetic impairment. To explore this causal relationship, we determined ATP levels and ATP/ADP ratio in DLP1 RNAi cells where MPP^+-induced mitochondrial fragmentation was blocked and found that the MPP^+-induced initial wave of rapid ATP or ATP/ADP ratio decline within the first hour was reduced and the second wave of decline was completely abolished in these cells. These results suggest that the initial drop in ATP levels is likely a direct effect of MPP^+ since MPP^+ is a selective inhibitor of complex I but that MPP^+-induced excessive mitochondrial fragmentation leads to further ATP decline, especially the second wave of ATP decline. This notion is consistent with prior studies demonstrating that excessive mitochondrial fragmentation leads to decreased ATP production mediated by increased ROS production and structural damage[32].

In our studies, we also found a biphasic pattern in ROS production and $[Ca^{2+}]_i$ induced by MPP^+ treatment. However, compared to MPP^+-induced mitochondrial fragmentation and ATP decline, a longer interval between the two waves of ROS production were noted, suggesting that they may be downstream events. Indeed, MPP^+-induced ROS production is completely abolished in DLP1 RNAi cells, suggesting that MPP^+-induced mitochondrial fragmentation mediates ROS production. This is consistent with recent studies demonstrating that mitochondrial fragmentation mediated by the fission process is a necessary component to ROS overproduction, and that cells with fragmented mitochondria demonstrate enhanced ROS production[13, 32–35]. Although it is unclear how enhanced mitochondrial fragmentation induces increased ROS production, it is possible that large-scale changes in the mitochondrial membranes during mitochondrial fragmentation causes structural derangement of electron transport chain (ETC) components residing on the inner mitochondrial membrane and leads to a perturbation of ETC activity and increased ROS production. Indeed, cells with fragmented mitochondria due to a deficiency in Mfn1/2 or OPA1 have greatly reduced endogenous and uncoupled respiratory rates caused by compromised electron transport in respiration complexes I, III, and IV[36, 37]. This said, it is also known that ROS can also lead to enhanced mitochondrial fragmentation[35, 38]. Indeed, in our studies, we found that NAC, a free radical scavenger which could almost completely prevent MPP^+-induced ROS production, also reduces MPP^+-induced mitochondrial fragmentation at later time points (i.e., second wave), confirming a crosstalk between mitochondrial fragmentation and ROS production induced by MPP^+ treatment. Such a crosstalk likely leads to a vicious downward spiral that augments the adverse effects of MPP^+. Because a fragmented mitochondrial network is less efficient in buffering changes in $[Ca^{2+}]_i$ due to the reduced overall volume and reduced connectivity of mitochondria[39] and because Ca^{2+} is functionally important in the control of mitochondrial dynamics through regulation of DLP1 phosphorylation and mitochondrial recruitment[40, 41], a similar crosstalk and vicious spiral may also be present between MPP^+-induced mitochondrial fragmentation and increased $[Ca^{2+}]_i$. This idea is supported by our findings showing that blocking mitochondrial fragmentation dampens the increase in $[Ca^{2+}]_i$. Additionally, D-AP5, a NMDA-receptor antagonist, blocks the second wave of $[Ca^{2+}]_i$ increase and alleviates MPP^+-induced mitochondrial fragmentation. It remains unclear what causes MPP^+-induced initial increases in $[Ca^{2+}]_i$ within the first hour.

We also measured MPP^+-induced changes in MMP and explored the temporal and functional relationship between MMP and mitochondrial fragmentation. While MPP^+ induces MMP decreases as early as 1 h, an effect that lasts for a prolonged period of time, this could be completely prevented by DLP1 knockdown suggesting that mitochondrial fragmentation is upstream of the MMP deficits and mediates MMP decline. This scheme is consistent with prior studies showing that excessive mitochondrial fission leads to reduced MMP while enhancing mitochondrial fusion can restore MMP[32]. Of note, prolonged and irreversible mitochondrial depolarization represents a critical step during excitotoxic cell death[42] such that decreasing MMP exacerbates MPP^+-induced apoptosis while enhancing MMP protects cells exposed to MPP^+. As such, while it is clear that MMP decline contributes to MPP^+-induced toxicity[43], our more detailed studies here also reveal that MPP^+ exposure causes acute mitochondrial effect (i.e., MMP reduction) within 1 h followed by more chronic toxicological effects (i.e., apoptosis) after 2–3 days[44], suggesting that the immediate mitochondrial effects are an accurate predictor of subsequent cell death. Therefore, although caspase 3 activation occurs after 24 h of MPP^+ treatment, much later than the initial MPP^+–induced MMP decline, it is still possible that decline in MMP contributes to MPP^+-induced apoptosis in our study because prolonged depolarization, even at a modest degree, would be sufficient to have substantial effects on the ability of mitochondria to accumulate calcium and sensitize neurons to increased ROS formation and

other excitotoxic insults[45]. In this regard, it is notable that MPP^+-induced ROS generation peaks around 24 hr of treatment when caspase 3 activation was first observed.

Consistent with prior studies[8], we found MPP^+ induced increases in autophagy/mitophagy. While changes in mitophagy could affect mitochondrial morphology[46], MPP^+ induced mitophagy occurs much later than MPP^+ induced mitochondrial fragmentation and could also be completely prevented by DLP1 knockdown, thus placing mitophagy downstream of mitochondrial fragmentation. This is consistent with the findings that excessive mitochondrial fission, caused by overexpression of fission protein Fis1, also induces mitophagy[47]. Although a temporally late event, it is perhaps not co-incident that MPP^+ induced autophagy/mitophagy was observed when significant cell death and caspase 3 cleavage occurred because it is not uncommon that multiple parallel cellular suicide mechanisms participate in neuronal death[48] and increased autophagy could promote cell death by regulating the mitochondria-mediated apoptotic pathway[49]. Moreover, neuronal lysosomes contain cathepsins B and L[50], which can activate caspase-3 during apoptosis in liver cells[51]. Indeed, inhibition of MPP^+ induced increased mitophagy could partially block MPP^+ induced cell death (not shown)[8], and hypoxic preconditioning inhibits MPP^+ induced cell death and caspase-3 activation by attenuating MPP^+ induced autophagy[52], suggesting that over-stimulated autophagy/mitophagy contributes to MPP^+ induced caspase activation and cell death. Although it is thought that MPP^+ induced autophagy/mitophagy is due to increased damage to organelles and mitochondrial-derived ROS are likely involved[53], the detailed mechanisms remain unclear. We found that a pan-caspase inhibitor, z-VAD-fmk, could partially reduce MPP^+ induced increases in the LC3-II/LC3-I ratio (not shown), indicating that caspase activation might play a role in MPP^+ induced mitophagy overactivation which is consistent with our finding that initial caspase activation occurs earlier than the induction of mitophagy. However, since some studies show that z-VAD-fmk can also inhibit a lysosomal protease and may directly interfere with the autophagic pathway[54], this finding should be cautiously interpreted.

In primary rat midbrain dopaminergic neurons, we found that 0.5 μM MPP^+ only induced mitochondrial fragmentation in TH-positive neurons but not in TH-negative neurons. This finding not only confirms that dopaminergic neurons are more sensitive to the effect of MPP^+, but also suggests that alterations of mitochondrial morphology are specific intracellular effects of MPP^+ in TH-positive neurons. Our time course study confirmed that, similar to SH-SY5Y cells, mitochondrial fragmentation is a very early event which suggests that it likely also mediates toxic effects induced by MPP^+ in primary TH-positive neurons. Interestingly, in addition to the rapid mitochondrial fragmentation, we also found that MPP^+ induces a biphasic decrease in mitochondrial coverage in neurites (i.e., decreased neurite mitochondrial index), which is likely due to a combined effect of reduced mitochondrial size and changes in mitochondrial numbers in neurites. One potential consequence of reduced mitochondrial coverage in neurites is synaptic dysfunction[13]. In this regard, it is of interest to note that loss of synaptic terminals in the striatum precedes loss of dopaminergic neurons in PD patients and in MPTP-treated mice[55, 56]. Our findings suggest that it is likely abnormal mitochondrial distribution, in addition to excessive mitochondrial fragmentation, that contributes to mitochondrial, synaptic, and neuronal dysfunction in MPP^+ models.

Overall, our findings indicate that MPP^+-induced DLP1-dependent mitochondrial fragmentation is an early event that works downstream or in parallel to MPP^+-induced bioenergetic dysfunction to mediate many adverse effects such as increased ROS production, decreased MMP, calcium disturbance, increased mitophagy and cell death in neuronal cells. A crosstalk between ROS and calcium disturbance and mitochondrial fragmentation form a mitochondrial fission-initiated downward spiral that augments these adverse effects.

Emerging evidence suggest that abnormal mitochondrial dynamics are involved in mitochondrial dysfunction critical for PD pathogenesis in PD patients and genetic models of PD. For example, mitochondrial morphology and function are impaired in fibroblasts or lymphocytes from PD patients carrying PINK1, Parkin or DJ-1 mutations[57–59]. DJ-1 knock-out mouse embryonic fibroblasts demonstrate reduced mitochondrial connectivity due to fragmentation which can be rescued by overexpression of wild type human DJ-1 PINK1 or Parkin[60]. Indeed, the PINK1/Parkin pathway promotes mitochondrial fission and/or inhibits mitochondrial fusion in Drosophila likely by mediating the ubiquitination of the profusion factor Mfn[14, 61–65]. In contrast, in mammalian cells, siRNA knockdown of PINK1 or Parkin leads to mitochondrial fragmentation[58, 64, 66] which is coordinated with enhanced mitochondrial turnover by autophagy[46]. DLP1 overexpression exacerbates the PINK1-deficiency phenotype while DLP1 knockdown or expression of dominant-negative DLP1 mutant rescues it[16]. Despite these discrepancies, it is apparent that PD-associated genes do play an essential role in the regulation of mitochondrial dynamics and quality control. Our findings presented here support the involvement of abnormal mitochondrial dynamics in a toxin model of PD. Therefore, alterations in mitochondrial dynamics are likely a common pathogenic pathway of PD and, as such, may represent a novel therapeutic target.

EXPERIMENTAL PROCEDURES

Cell culture and transfection

Human SH-SY5Y neuroblastoma cell lines were grown in Opti-MEM I medium (Invitrogen) supplemented with 10% (v/v) fetal bovine serum and 1% penicillin-streptomycin, in 5% CO_2 in a humid incubator at 37°C. Cells were transfected using Effectene (QIAGEN) according to the manufacturer's instructions. For co-transfection, a 3:1 ratio of indicated plasmid: mito-DsRed2 was used. Culture medium containing 20 μg/ml Blasticidin (Invitrogen) was used for the selection of stable cell lines. The selection medium was replaced every 3 days until the appearance of foci, each apparently derived from a single stably transfected cell. Stable cell lines were then picked and maintained with 5 μg/ml Blasticidin. Some cultures received treatment of E64 (10 μg/ml) (Sigma) and pepstatin A (10 μg/ml) (Sigma) for 48 h to inhibit lysosomal degradation.

Primary neurons from E18 rat ventral midbrain tissue (BrainBits) were seeded at 50,000–60,000 cells per well on 8-well chamber slides coated with Poly-D-Lysine/Laminin (BD) in neurobasal medium supplemented with 2% B27 (Invitrogen) and 0.5 mM glutamine. Half the culture medium was changed after 3 days with neurobasal medium supplemented with 2% B27 (Invitrogen), 0.5 mM glutamine and 2 uM cytosine arabinoside to inhibit glial proliferation. At 6 days in vitro (DIV), cells were treated with 0.5 μM MPP^+ for various periods of time up to 24 hr. All cultures were kept at 37°C in a humidified 5% CO_2 containing atmosphere.

Plasmids, antibodies and chemicals

Mito-DsRed2 construct (Clontech), GFP tagged wild type DLP1/mutant DLP1 K38A/Fis1 constructs (gifts from Dr. Yisang Yoon, University of Rochester), GFP tagged LC3 (gift from Dr. Noboru Mizushima, Tokyo Medical and Dental University, Japan) and Case12 construct (Evrogen) were used. The miR RNAi vector was generated with the pcDNA 6.2-GW/EmGFP-miR construct (Invitrogen). The miR RNAi sequence targeting the open reading frame region of human DLP1 was described previously[35]. The negative control RNAi plasmid contains a scrambled sequence that did not target any known vertebrate gene. Primary antibodies used included mouse anti-DLP1 (BD Biosciences), mouse anti-GAPDH and Actin and rabbit anti-calnexin (Chemicon), rabbit anti-α-tubulin (Epitomics), rabbit anti-LC3 (MBL International) and rabbit anti- COX IV and LC3 (Cell Signaling), rabbit anti-

tyrosine hydroxylase (Calbiochem). 1-methyl-4-phenylpyridinium,N-Acetyl-L-cysteine (Sigma) and D-AP5 (Tocris) were also used.

Western blot analysis

Cells were lysed with Cell Lysis Buffer (Cell Signaling) containing 1 mM PMSF (Sigma) and Protease Inhibitor Cocktail (Sigma). Equal amounts of total protein extract were resolved by SDS-PAGE and transferred to Immobilon-P (Millipore). Following blocking with 10% nonfat dry milk, primary and secondary antibodies were applied as previously described[35] and the blots developed with Immobilon Western Chemiluminescent HRP Substrate (Millipore).

Cell measurements

Cell death and viability was measured by Cytotoxicity Detection Kit (LDH; Roche) and Cell Proliferation Kit (MTT; Roche) respectively. ATP levels were measured by the ATP Determination Kit according to manufacturer's instructions (Invitrogen), ATP/ADP ratio by ApoSENSOR™ ADP/ATP Ratio Assay Kit (Biovision) according to manufacturer's instructions. All measurements were normalized to protein content measured by BCA protein assay (Pierce).

The ROS level and mitochondrial membrane potential was measured as previously described[32]. ROS level was measured by H2DCFDA (Invitrogen), Plasma membrane potential (PMP) by bis-(1,3-dibutylbarbituric acid) pentamethine oxonol (DiBAC4(5), Invitrogen), mitochondria membrane potential (MMP) by TMRM (Invitrogen) according to manufacturer's instructions. All these measurements were normalized to cell number counted by hemocytometer. Mitochondria were isolated from cells using a mitochondrial isolation kit (Pierce) following the manufacturer's protocol.

Immunofluorescence and quantification of mitochondrial morphology

Cells were seeded on 4 well chamber slides. After treatment, cells were fixed and stained as described previously[35]. All fluorescence images were captured with a Zeiss LSM 510 inverted fluorescence microscope or a Zeiss LSM 510 inverted laser-scanning confocal fluorescence microscope as described before[35]. Image analysis was performed with open-source image-analysis programs WCIF ImageJ (developed by W. Rasband). For SH-SY5Y cells, mitochondria morphology were quantified as described before[67]. Taken briefly, raw images were background corrected, linearly contrast optimized, applied with a 7×7 “top hat” filter, subjected to a 3×3 median filter and then thresholded to generate binary images. Most mitochondria were well separately in binary images and thus big clustering of mitochondria were excluded automatically. All binary images were analyzed by Image J to provide information of mitochondria aspect ratio (ratio between major and minor axes of an ellipse equivalent to the mitochondrion), which was a relative measure of mitochondrial length. Because the automatic manipulation of the raw image may slightly change both the length and width of individual mitochondrion, the aspect ratio is a better index for mitochondrial morphology. For primary neurons, mitochondria are well separated from each other, making it possible to measure mitochondria length directly from raw pictures. Raw confocal or fluorescent images were background corrected and then directly analyzed by Image J to provide the absolute measurement of mitochondria length.

Time-lapse imaging

Cells were seeded in glass-bottomed dishes (MatTek) and then transfected with mito-DsRed2 or Case12. Forty-eight (48) h after transfection, cells were put in a well-equipped environmental chamber with controlled CO_2 content, humidity and temperature and imaged

by an inverted Leica DMI6000 fluorescence microscope (Leica) as previously described[18]. Images were acquired every 5 or 10 min. Image analysis was also performed with WCIF ImageJ (developed by W. Rasband) and MetaMorph Software (Version 7.04, Molecular Devices).

Acknowledgments

This study is supported by the NIH (NS071184) and American Parkinson Disease Association.

REFERENCES

1. Lesage S, Brice A. Parkinson's disease: from monogenic forms to genetic susceptibility factors. Hum Mol Genet. 2009; 18:R48–59. [PubMed: 19297401]
2. Przedborski S, Vila M. The 1-methyl-4-phenyl-1,2,3,6-tetrahydropyridine mouse model: a tool to explore the pathogenesis of Parkinson's disease. Ann N Y Acad Sci. 2003; 991:189–198. [PubMed: 12846987]
3. Henchcliffe C, Beal MF. Mitochondrial biology and oxidative stress in Parkinson disease pathogenesis. Nat Clin Pract Neurol. 2008; 4:600–609. [PubMed: 18978800]
4. Swerdlow RH, Parks JK, Miller SW, Tuttle JB, Trimmer PA, Sheehan JP, Bennett JP Jr. Davis RE, Parker WD Jr. Origin and functional consequences of the complex I defect in Parkinson's disease. Ann Neurol. 1996; 40:663–671. [PubMed: 8871587]
5. Bindoff LA, Birch-Machin M, Cartlidge NE, Parker WD Jr. Turnbull DM. Mitochondrial function in Parkinson's disease. Lancet. 1989; 2:49. [PubMed: 2567823]
6. Keeney PM, Xie J, Capaldi RA, Bennett JP Jr. Parkinson's disease brain mitochondrial complex I has oxidatively damaged subunits and is functionally impaired and misassembled. J Neurosci. 2006; 26:5256–5264. [PubMed: 16687518]
7. Przedborski S, Jackson-Lewis V. Mechanisms of MPTP toxicity. Mov Disord. 1998; 13(Suppl 1): 35–38. [PubMed: 9613716]
8. Zhu JH, Horbinski C, Guo F, Watkins S, Uchiyama Y, Chu CT. Regulation of autophagy by extracellular signal-regulated protein kinases during 1-methyl-4-phenylpyridinium-induced cell death. Am J Pathol. 2007; 170:75–86. [PubMed: 17200184]
9. Chen H, Chan DC. Critical dependence of neurons on mitochondrial dynamics. Curr Opin Cell Biol. 2006; 18:453–459. [PubMed: 16781135]
10. Smirnova E, Shurland DL, Ryazantsev SN, van der Bliek AM. A human dynamin-related protein controls the distribution of mitochondria. J Cell Biol. 1998; 143:351–358. [PubMed: 9786947]
11. Cipolat S, Martins de Brito O, Dal Zilio B, Scorrano L. OPA1 requires mitofusin 1 to promote mitochondrial fusion. Proc Natl Acad Sci U S A. 2004; 101:15927–15932. [PubMed: 15509649]
12. Detmer SA, Chan DC. Functions and dysfunctions of mitochondrial dynamics. Nat Rev Mol Cell Biol. 2007; 8:870–879. [PubMed: 17928812]
13. Wang X, Su B, Lee HG, Li X, Perry G, Smith MA, Zhu X. Impaired balance of mitochondrial fission and fusion in Alzheimer's disease. J Neurosci. 2009; 29:9090–9103. [PubMed: 19605646]
14. Poole AC, Thomas RE, Andrews LA, McBride HM, Whitworth AJ, Pallanck LJ. The PINK1/Parkin pathway regulates mitochondrial morphology. Proc Natl Acad Sci U S A. 2008; 105:1638–1643. [PubMed: 18230723]
15. Liot G, Bossy B, Lubitz S, Kushnareva Y, Sejbuk N, Bossy-Wetzel E. Complex II inhibition by 3-NP causes mitochondrial fragmentation and neuronal cell death via an NMDA- and ROS-dependent pathway. Cell Death Differ. 2009; 16:899–909. [PubMed: 19300456]
16. Sandebring A, Thomas KJ, Beilina A, van der Brug M, Cleland MM, Ahmad R, Miller DW, Zambrano I, Cowburn RF, Behbahani H, Cedazo-Minguez A, Cookson MR. Mitochondrial alterations in PINK1 deficient cells are influenced by calcineurin-dependent dephosphorylation of dynamin-related protein 1. PLoS One. 2009; 4:e5701. [PubMed: 19492085]
17. Gomez-Lazaro M, Bonekamp NA, Galindo MF, Jordan J, Schrader M. 6-Hydroxydopamine (6-OHDA) induces Drp1-dependent mitochondrial fragmentation in SH-SY5Y cells. Free Radic Biol Med. 2008; 44:1960–1969. [PubMed: 18395527]

18. Yoon Y, Pitts KR, Dahan S, McNiven MA. A novel dynamin-like protein associates with cytoplasmic vesicles and tubules of the endoplasmic reticulum in mammalian cells. J Cell Biol. 1998; 140:779–793. [PubMed: 9472031]

19. Klionsky DJ, Abeliovich H, Agostinis P, Agrawal DK, Aliev G, Askew DS, Baba M, Baehrecke EH, Bahr BA, Ballabio A, Bamber BA, Bassham DC, Bergamini E, Bi XN, Biard-Piechaczyk M, Blum JS, Breclesen DE, Brodsky JL, Brumell JH, Brunk UT, Bursch W, Camougrand N, Cebollero E, Cecconi F, Chen YY, Chin LS, Choi A, Chu CT, Chung JK, Clarke PGH, Clark RSB, Clarke SG, Clave C, Cleveland JL, Codogno P, Colombo MI, Coto-Montes A, Cregg JM, Cuervo AM, Debnath J, Demarchi F, Dennis PB, Dennis PA, Deretic V, Devenish RJ, Di Sano F, Dice JF, DiFiglia M, Dinesh-Kumar S, Distelhorst CW, Djavaheri-Mergny M, Dorsey FC, Droge W, Dron M, Dunn WA, Duszenko M, Eissa NT, Elazar Z, Esclatine A, Eskelinen EL, Fesues L, Finley KD, Fuentes JM, Fueyo J, Fujisaki K, Galliot B, Gao FB, Gewirtz DA, Gibson SB, Gohla A, Goldberg AL, Gonzalez R, Gonzalez-Estevez C, Gorski S, Gottlieb RA, Haussinger D, He YW, Heidenreich K, Hill JA, Hoyer-Hansen M, Hu X, Huang WP, Iwasaki A, Jaattela M, Jackson WT, Jiang X, Jin SK, Johansen T, Jung JU, Kadowaki M, Kang C, Kelekar A, Kessel DH, Kiel JAKW, Kim HP, Kimchi A, Kinsella TJ, Kiselyov K, Kitamoto K, Knecht E, Komatsu M, Kominami E, Konclo S, Kovacs AL, Kroemer G, Kuan CY, Kumar R, Kundu M, Landry J, Laporte M, Le WD, Lei HY, Lenardo MJ, Levine B, Lieberman A, Lim KL, Lin FC, Liou W, Liu LF, Lopez-Berestein G, Lopez-Otin C, Lu B, Macleod KF, Malorni W, Martinet W, Matsuoka K, Mautner J, Meijer AJ, Melendez A, Michels P, Miotto G, Mistiaen WP, Mizushima N, Mograbi B, Monastyrska I, Moore MN, Moreira PI, Moriyasu Y, Motyl T, Munz C, Murphy LO, Naqvi NI, Neufeld TP, Nishino I, Nixon RA, Noda T, Nurnberg B, Ogawa M, Oleinick NL, Olsen LJ, Ozpolat B, Paglin S, Palmer GE, Papassideri I, Parkes M, Perlmutter DH, Perry G, Piacentini M, Pinkas-Kramarski R, Prescott M, Proikas-Cezanne T, Raben N, Rami A, Reggiori F, Rohrer B, Rubinsztein DC, Ryan KM, Sadoshima J, Sakagami H, Sakai Y, Sandri M, Sasakawa C, Sass M, Schneider C, Seglen PO, Seleverstov O, Settleman J, Shacka JJ, Shapiro IM, Sibirny A, Silva-Zacarin ECM, Simon HU, Simone C, Simonsen A, Smith MA, Spanel-Borowski K, Srinivas V, Steeves M, Stenmark H, Stromhaug PE, Subauste CS, Sugimoto S, Sulzer D, Suzuki T, Swanson MS, Takeshita F, Talbot NJ, Talloczy Z, Tanaka K, Tanaka K, Tanida I, Taylor GS, Taylor JP, Terman A, Tettamanti G, Thompson CB, Thumm M, Tolkovsky AM, Tooze SA, Truant R, Tumanovska LV, Uchiyama Y, Ueno T, Uzcategui NL, van der Klei I, Vaquero EC, Vellai T, Vogel MW, Wang HG, Webster P, Wiley JW, Xi ZJ, Xiao G, Yahalom J, Yang JM, Yap G, Yin XM, Yoshimori T, Yu L, Yue ZY, Yuzaki M, Zabirnyk O, Zheng XX, Zhu X, Deter RL, Tabas I. Guidelines for the use and interpretation of assays for monitoring autophagy in higher eukaryotes. Autophagy. 2008; 4:151–175. [PubMed: 18188003]

20. Kim I, Rodriguez-Enriquez S, Lemasters JJ. Selective degradation of mitochondria by mitophagy. Arch Biochem Biophys. 2007; 462:245–253. [PubMed: 17475204]

21. Mizushima N, Yamamoto A, Hatano M, Kobayashi Y, Kabeya Y, Suzuki K, Tokuhisa T, Ohsumi Y, Yoshimori T. Dissection of autophagosome formation using Apg5-deficient mouse embryonic stem cells. Journal of Cell Biology. 2001; 152:657–667. [PubMed: 11266458]

22. Lee DH, Han YS, Han ES, Bang H, Lee CS. Differential involvement of intracellular Ca2+ in 1-methyl-4-phenylpyridinium- or 6-hydroxydopamine-induced cell viability loss in PC12 cells. Neurochem Res. 2006; 31:851–860. [PubMed: 16804760]

23. Camins A, Sureda FX, Gabriel C, Pallas M, Escubedo E, Camarasa J. Effect of 1-methyl-4-phenylpyridinium (MPP+) on mitochondrial membrane potential in cerebellar neurons: interaction with the NMDA receptor. J Neural Transm. 1997; 104:569–577. [PubMed: 9444558]

24. Kang HT, Hwang ES. Nicotinamide enhances mitochondria quality through autophagy activation in human cells. Aging Cell. 2009; 8:426–438. [PubMed: 19473119]

25. Sauvanet C, Duvezin-Caubet S, di Rago JP, Rojo M. Energetic requirements and bioenergetic modulation of mitochondrial morphology and dynamics. Semin Cell Dev Biol. 2010; 21:558–565. [PubMed: 20025987]

26. Choi WS, Kruse SE, Palmiter RD, Xia Z. Mitochondrial complex I inhibition is not required for dopaminergic neuron death induced by rotenone, MPP+, or paraquat. Proc Natl Acad Sci U S A. 2008; 105:15136–15141. [PubMed: 18812510]

27. Yonashiro R, Ishido S, Kyo S, Fukuda T, Goto E, Matsuki Y, Ohmura-Hoshino M, Sada K, Hotta H, Yamamura H, Inatome R, Yanagi S. A novel mitochondrial ubiquitin ligase plays a critical role in mitochondrial dynamics. EMBO J. 2006; 25:3618–3626. [PubMed: 16874301]

28. Caneda-Ferron B, De Girolamo LA, Costa T, Beck KE, Layfield R, Billett EE. Assessment of the direct and indirect effects of MPP+ and dopamine on the human proteasome: implications for Parkinson's disease aetiology. J Neurochem. 2008; 105:225–238. [PubMed: 18021296]

29. Domingues AF, Arduino DM, Esteves AR, Swerdlow RH, Oliveira CR, Cardoso SM. Mitochondria and ubiquitin-proteasomal system interplay: relevance to Parkinson's disease. Free Radic Biol Med. 2008; 45:820–825. [PubMed: 18619530]

30. Cheng YF, Zhu GQ, Wang M, Cheng H, Zhou A, Wang N, Fang N, Wang XC, Xiao XQ, Chen ZW, Li QL. Involvement of ubiquitin proteasome system in protective mechanisms of Puerarin to MPP(+)-elicited apoptosis. Neurosci Res. 2009; 63:52–58. [PubMed: 19022306]

31. Estaquier J, Arnoult D. Inhibiting Drp1-mediated mitochondrial fission selectively prevents the release of cytochrome c during apoptosis. Cell Death Differ. 2007; 14:1086–1094. [PubMed: 17332775]

32. Wang X, Su B, Siedlak SL, Moreira PI, Fujioka H, Wang Y, Casadesus G, Zhu X. Amyloid-beta overproduction causes abnormal mitochondrial dynamics via differential modulation of mitochondrial fission/fusion proteins. Proc Natl Acad Sci U S A. 2008; 105:19318–19323. [PubMed: 19050078]

33. Yu T, Robotham JL, Yoon Y. Increased production of reactive oxygen species in hyperglycemic conditions requires dynamic change of mitochondrial morphology. Proc Natl Acad Sci U S A. 2006; 103:2653–2658. [PubMed: 16477035]

34. Yu T, Sheu SS, Robotham JL, Yoon Y. Mitochondrial fission mediates high glucose-induced cell death through elevated production of reactive oxygen species. Cardiovasc Res. 2008; 79:341–351. [PubMed: 18440987]

35. Wang X, Su B, Fujioka H, Zhu X. Dynamin-like protein 1 reduction underlies mitochondrial morphology and distribution abnormalities in fibroblasts from sporadic Alzheimer's disease patients. Am J Pathol. 2008; 173:470–482. [PubMed: 18599615]

36. Chen H, Chomyn A, Chan DC. Disruption of fusion results in mitochondrial heterogeneity and dysfunction. J Biol Chem. 2005; 280:26185–26192. [PubMed: 15899901]

37. Chen H, Detmer SA, Ewald AJ, Griffin EE, Fraser SE, Chan DC. Mitofusins Mfn1 and Mfn2 coordinately regulate mitochondrial fusion and are essential for embryonic development. J Cell Biol. 2003; 160:189–200. [PubMed: 12527753]

38. Pletjushkina OY, Lyamzaev KG, Popova EN, Nepryakhina OK, Ivanova OY, Domnina LV, Chernyak BV, Skulachev VP. Effect of oxidative stress on dynamics of mitochondrial reticulum. Biochim Biophys Acta. 2006; 1757:518–524. [PubMed: 16829229]

39. Frieden M, James D, Castelbou C, Danckaert A, Martinou JC, Demaurex N. Ca(2+) homeostasis during mitochondrial fragmentation and perinuclear clustering induced by hFis1. J Biol Chem. 2004; 279:22704–22714. [PubMed: 15024001]

40. Cereghetti GM, Stangherlin A, Martins de Brito O, Chang CR, Blackstone C, Bernardi P, Scorrano L. Dephosphorylation by calcineurin regulates translocation of Drp1 to mitochondria. Proc Natl Acad Sci U S A. 2008; 105:15803–15808. [PubMed: 18838687]

41. Han XJ, Lu YF, Li SA, Kaitsuka T, Sato Y, Tomizawa K, Nairn AC, Takei K, Matsui H, Matsushita M. CaM kinase I alpha-induced phosphorylation of Drp1 regulates mitochondrial morphology. J Cell Biol. 2008; 182:573–585. [PubMed: 18695047]

42. Abramov AY, Duchen MR. Mechanisms underlying the loss of mitochondrial membrane potential in glutamate excitotoxicity. Biochim Biophys Acta. 2008; 1777:953–964. [PubMed: 18471431]

43. Selvaraj S, Watt JA, Singh BB. TRPC1 inhibits apoptotic cell degeneration induced by dopaminergic neurotoxin MPTP/MPP(+). Cell Calcium. 2009; 46:209–218. [PubMed: 19695701]

44. Stephans SE, Miller GW, Levey AI, Greenamyre JT. Acute mitochondrial and chronic toxicological effects of 1-methyl-4-phenylpyridinium in human neuroblastoma cells. Neurotoxicology. 2002; 23:569–580. [PubMed: 12428729]

45. Nicholls D, Akerman K. Mitochondrial calcium transport. Biochim Biophys Acta. 1982; 683:57–88. [PubMed: 6291604]

46. Dagda RK, Cherra SJ 3rd, Kulich SM, Tandon A, Park D, Chu CT. Loss of PINK1 function promotes mitophagy through effects on oxidative stress and mitochondrial fission. J Biol Chem. 2009; 284:13843–13855. [PubMed: 19279012]
47. Gomes LC, Scorrano L. High levels of Fis1, a pro-fission mitochondrial protein, trigger autophagy. Biochim Biophys Acta. 2008; 1777:860–866. [PubMed: 18515060]
48. Lohr HR, Kuntchithapautham K, Sharma AK, Rohrer B. Multiple, parallel cellular suicide mechanisms participate in photoreceptor cell death. Exp Eye Res. 2006; 83:380–389. [PubMed: 16626700]
49. Wang Y, Han R, Liang ZQ, Wu JC, Zhang XD, Gu ZL, Qin ZH. An autophagic mechanism is involved in apoptotic death of rat striatal neurons induced by the non-N-methyl-D-aspartate receptor agonist kainic acid. Autophagy. 2008; 4:214–226. [PubMed: 18094625]
50. Bernstein HG, Sormunen R, Jarvinen M, Kloss P, Kirschke H, Rinne A. Cathepsin B immunoreactive neurons in rat brain. A combined light and electron microscopic study. J Hirnforsch. 1989; 30:313–317. [PubMed: 2745967]
51. Vancompernolle K, Van Herreweghe F, Pynaert G, Van de Craen M, De Vos K, Totty N, Sterling A, Fiers W, Vandenabeele P, Grooten J. Atractyloside-induced release of cathepsin B, a protease with caspase-processing activity. FEBS Lett. 1998; 438:150–158. [PubMed: 9827536]
52. Tzeng YW, Lee LY, Chao PL, Lee HC, Wu RT, Lin AM. Role of autophagy in protection afforded by hypoxic preconditioning against MPP+-induced neurotoxicity in SH-SY5Y cells. Free Radic Biol Med. 2010; 49:839–846. [PubMed: 20541008]
53. Chen Y, Gibson SB. Is mitochondrial generation of reactive oxygen species a trigger for autophagy? Autophagy. 2008; 4:246–248. [PubMed: 18094624]
54. Wu YT, Tan HL, Huang Q, Kim YS, Pan N, Ong WY, Liu ZG, Ong CN, Shen HM. Autophagy plays a protective role during zVAD-induced necrotic cell death. Autophagy. 2008; 4:457–466. [PubMed: 18253089]
55. Bernheimer H, Birkmayer W, Hornykiewicz O, Jellinger K, Seitelberger F. Brain dopamine and the syndromes of Parkinson and Huntington. Clinical, morphological and neurochemical correlations. J Neurol Sci. 1973; 20:415–455. [PubMed: 4272516]
56. Cochiolo JA, Ehsanian R, Bruck DK. Acute ultrastructural effects of MPTP on the nigrostriatal pathway of the C57BL/6 adult mouse: evidence of compensatory plasticity in nigrostriatal neurons. J Neurosci Res. 2000; 59:126–135. [PubMed: 10658193]
57. Mortiboys H, Thomas KJ, Koopman WJ, Klaffke S, Abou-Sleiman P, Olpin S, Wood NW, Willems PH, Smeitink JA, Cookson MR, Bandmann O. Mitochondrial function and morphology are impaired in parkin-mutant fibroblasts. Ann Neurol. 2008; 64:555–565. [PubMed: 19067348]
58. Exner N, Treske B, Paquet D, Holmstrom K, Schiesling C, Gispert S, Carballo-Carbajal I, Berg D, Hoepken HH, Gasser T, Kruger R, Winklhofer KF, Vogel F, Reichert AS, Auburger G, Kahle PJ, Schmid B, Haass C. Loss-of-function of human PINK1 results in mitochondrial pathology and can be rescued by parkin. J Neurosci. 2007; 27:12413–12418. [PubMed: 17989306]
59. Grunewald A, Gegg ME, Taanman JW, King RH, Kock N, Klein C, Schapira AH. Differential effects of PINK1 nonsense and missense mutations on mitochondrial function and morphology. Exp Neurol. 2009; 219:266–273. [PubMed: 19500570]
60. Blackinton J, Lakshminarasimhan M, Thomas KJ, Ahmad R, Greggio E, Raza AS, Cookson MR, Wilson MA. Formation of a Stabilized Cysteine Sulfinic Acid Is Critical for the Mitochondrial Function of the Parkinsonism Protein DJ-1. J Biol Chem. 2009; 284:6476–6485. [PubMed: 19124468]
61. Ziviani E, Tao RN, Whitworth AJ. Drosophila parkin requires PINK1 for mitochondrial translocation and ubiquitinates mitofusin. Proc Natl Acad Sci U S A. 2010; 107:5018–5023. [PubMed: 20194754]
62. Poole AC, Thomas RE, Yu S, Vincow ES, Pallanck L. The mitochondrial fusion-promoting factor mitofusin is a substrate of the PINK1/parkin pathway. PLoS One. 2010; 5:e10054. [PubMed: 20383334]
63. Deng H, Dodson MW, Huang H, Guo M. The Parkinson's disease genes pink1 and parkin promote mitochondrial fission and/or inhibit fusion in Drosophila. Proc Natl Acad Sci U S A. 2008; 105:14503–14508. [PubMed: 18799731]

64. Park J, Lee G, Chung J. The PINK1-Parkin pathway is involved in the regulation of mitochondrial remodeling process. Biochem Biophys Res Commun. 2009; 378:518–523. [PubMed: 19056353]

65. Yang Y, Ouyang Y, Yang L, Beal MF, McQuibban A, Vogel H, Lu B. Pink1 regulates mitochondrial dynamics through interaction with the fission/fusion machinery. Proc Natl Acad Sci U S A. 2008; 105:7070–7075. [PubMed: 18443288]

66. Lutz AK, Exner N, Fett ME, Schlehe JS, Kloos K, Laemmermann K, Brunner B, Kurz-Drexler A, Vogel F, Reichert AS, Bouman L, Vogt-Weisenhorn D, Wurst W, Tatzelt J, Haass C, Winklhofer KF. Loss of parkin or PINK1 function increases DRP1-dependent mitochondrial fragmentation. J Biol Chem. 2009; 284:22938–51. [PubMed: 19546216]

67. Koopman WJ, Distelmaier F, Esseling JJ, Smeitink JA, Willems PH. Computer-assisted live cell analysis of mitochondrial membrane potential, morphology and calcium handling. Methods. 2008; 46:304–311. [PubMed: 18929665]

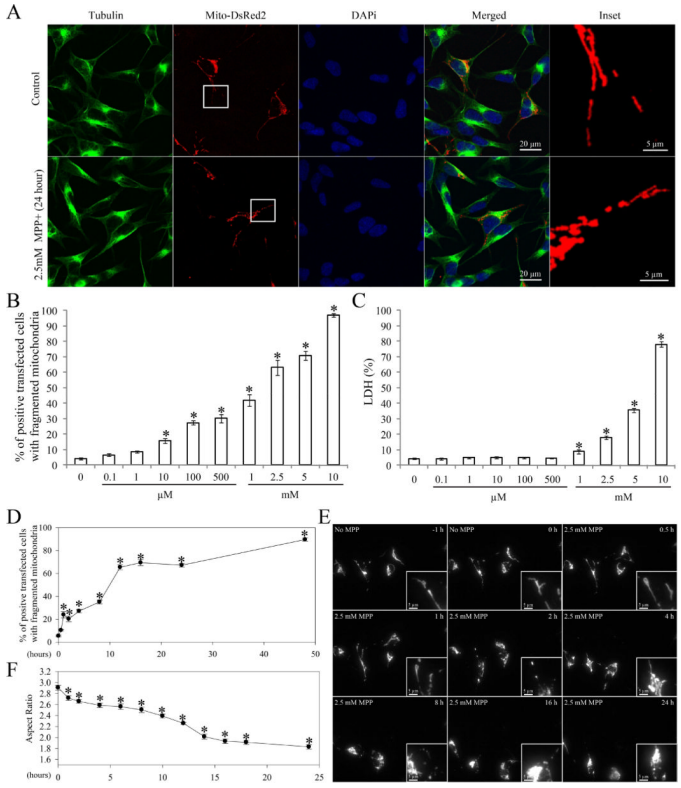

Figure 1. MPP$^+$ Induced Mitochondrial Fragmentation in SH-SY5Y Cells

SH-SY5Y cells were transfected with mito-DsRed2 to label mitochondria. Two days after transfection, cells were treated with different concentrations of MPP$^+$ (0.1 μM~10 mM) for 24 h or with 2.5 mM MPP$^+$ for different time points, fixed, immunostained with tubulin and evaluated. Representative pictures (A) of positively transfected cells treated with or without 2.5 mM MPP$^+$ for 24 h are shown. Green: Tubulin, Red: mito-DsRed2, Blue: DAPi. (B) Quantification of mitochondria morphology in SH-SY5Y cells treated with different concentrations of MPP$^+$ treatment for 24 h. (C) The LDH release assay was performed to evaluate cell death induced by MPP$^+$ treatment for 24 h. (D) Quantification of mitochondria morphology in fixed SH-SY5Y cells treated with 2.5 mM MPP$^+$ at different time points. (E) Representative time lapse pictures of mitochondria in live SH-SY5Y cells treated with 2.5 mM MPP$^+$. (F) Quantification of mitochondria morphology in live individual cells with fragmented mitochondria at different time points after 2.5 mM MPP$^+$ treatment (the aspect ratio of a mitochondrion is a ratio between the major and the minor axes of the ellipse equivalent to the mitochondria). At least 500 fixed cells or 20 live cells were analyzed in each experiment and experiments were repeated three times. (*p<0.05, when compared with the control cells without MPP$^+$ treatment; student-t-test.).

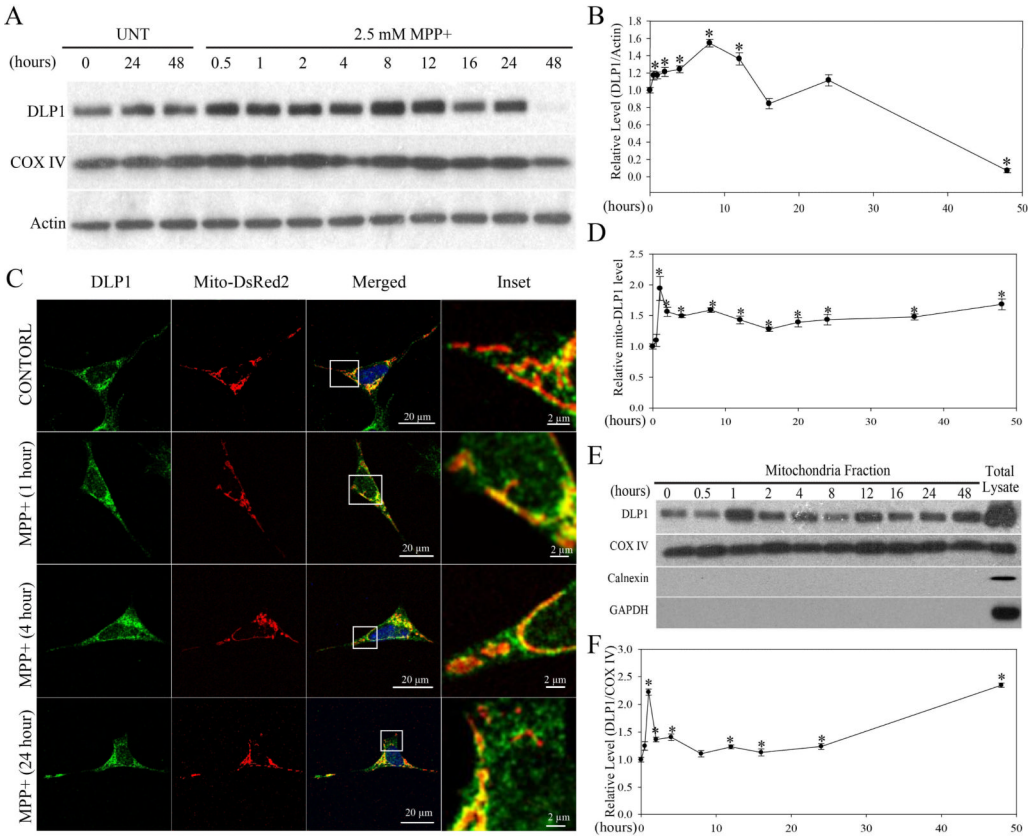

Figure 2. MPP$^+$ Induced Increased DLP1 Expression and Mitochondria Recruitment

Representative immunoblot (A) and quantification analysis (B) of the expression levels of DLP1 in SH-SY5Y cells treated with 2.5 mM MPP$^+$ up to 48 h. Equal protein amounts (10 μg) were loaded and confirmed with actin staining. (C) Representative immunofluorescence pictures demonstrate increased mitochondrial localization of DLP1 after treatment with 2.5 mM MPP$^+$. Green: DLP1, Red: mito-DsRed, Blue: DAPi. (D) Quantification of the immunoreactivity of DLP1 localized to mitochondria. The relative mito-DLP1 level was defined as the relative ratio (control is set as 1) between the intensity of green signal that co-localizes with red signal and the intensity of total red signal. At least 20 cells were analyzed in each experiment. (E) and (F) are representative immunoblot and quantification of the relative level of DLP1 in the mitochondria fraction from SH-SY5Y cells treated with 2.5 mM MPP$^+$ at different time points. All samples were also immunoblotted with antibodies to detect mitochondrial (COX IV), cytoplasmic (GAPDH) and endoplasmic reticulum (Calnexin) markers. The absence of GAPDH and Calnexin confirms the purity of the mitochondrial fraction preparations. All experiments were repeated three times. (*p<0.05, when compared with the control cells without MPP$^+$ treatment; student-t-test.).

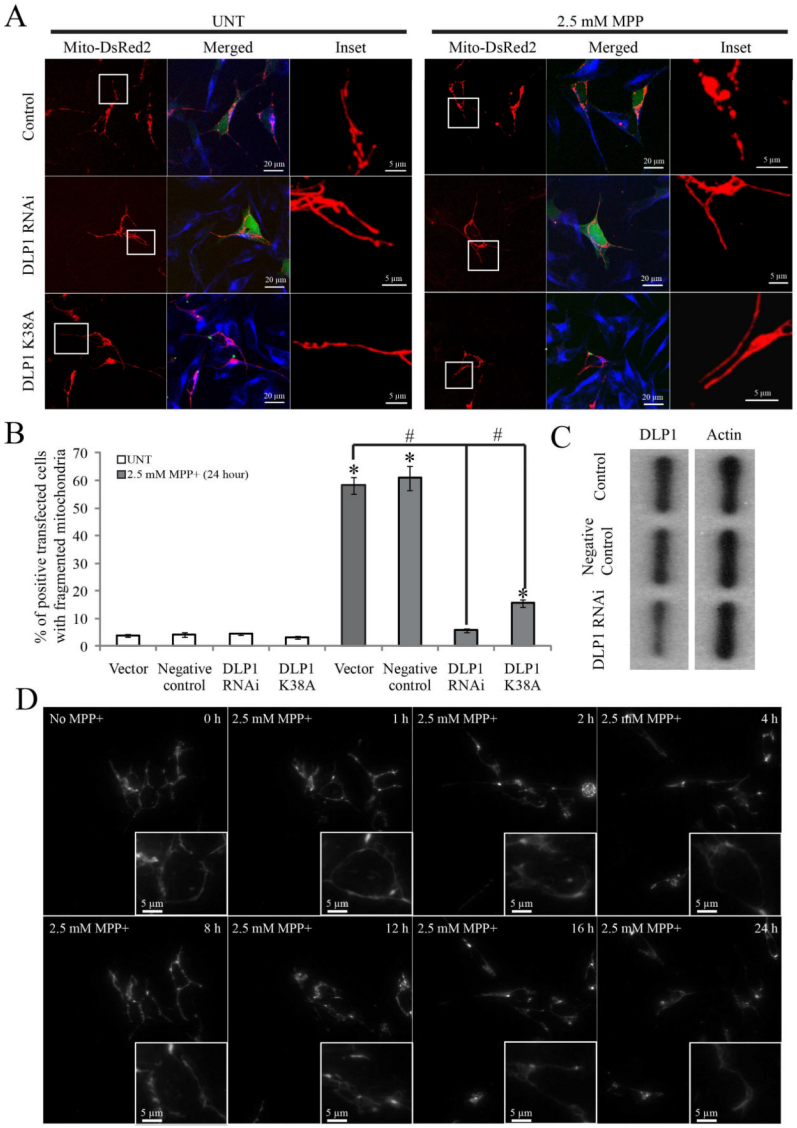

Figure 3. MPP$^+$-Induced Mitochondrial Fission Was Completely Abolished by Genetic Inactivation of DLP1

SH-SY5Y cells were co-transfected with GFP-tagged DLP1 RNAi constructs (DLP1 RNAi) or GFP-tagged dominant-negative mutant DLP1(DLP1 K38A) together with mito-DsRed2. Two days after transfection, cells were treated with 2.5 mM MPP$^+$ for 24 h, fixed, stained and analyzed. Representative pictures (A) and quantification analysis (B) show that both DLP1 knockdown or overexpression of DLP1 K38A mutant prevents mitochondrial fragmentation induced by 24 h treatment of 2.5 mM MPP$^+$. At least 500 cells were analyzed in each experiment. Red: mito-DsRed, Green: GFP, Blue: tubulin. (C) Representative immunoblot demonstrates recued DLP1 expression in SH-SY5Y cells transfected with GFP-tagged DLP1 RNAi. Equal protein amounts (10 μg) were loaded. Actin immunoblotting was used as an internal loading control. (D) Representative time lapse pictures of live SH-SY5Y cells positively transfected with DLP1 RNAi in the presence of 2.5 mM MPP$^+$ demonstrates no mitochondrial fragmentation up to 24 h. All experiments were repeated three times. (*p<0.05, when compared with the control cells without MPP$^+$ treatment; #p<0.05, when compared with control cells with MPP$^+$ treatment; student-t-test).

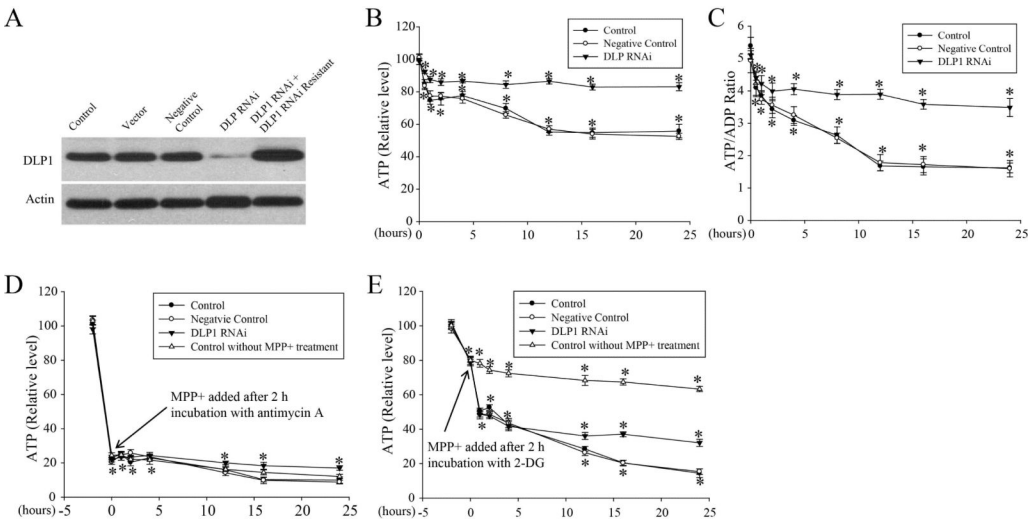

Figure 4. MPP^+ caused a rapid decrease in intracellular ATP levels and ATP/ADP ratio concurrent with enhanced mitochondrial fragmentation

(A) Representative immunoblot of DLP1 demonstrates reduced DLP1 expression in SH-SY5Y stable cell line transfected with GFP-tagged DLP1 RNAi constructs. Expression of RNAi resistant DLP1 restores DLP1 levels in these cell lines. Equal protein amounts (10 μg) were loaded and actin was used as an internal loading control. (B–C) SH-SY5Y cells (control: wild type cells; Negative control: cell lines expressing scrambled RNAi negative-control vector; DLP1 RNAi: cell lines expressing DLP1 RNAi vector) seeded on 96 well plates were treated with 2.5 mM MPP^+ and intracellular ATP levels (B) and ATP/ADP ratio (C) were measured after various incubation times. All experiments were repeated three times (*p<0.05, when compared with each cell line without MPP^+ treatment; student-t-test). (D–E) SH-SY5Y cells (control: wild type cells; Negative control: cell lines expressing scrambled RNAi negative-control vector; DLP1 RNAi: cell lines expressing DLP1 RNAi vector) seeded on 96 well plates were pre-incubated with 5 μM antimycin A (D) or 1 mM 2-deoxyglucose (E) for 2 hrs, and then treated with 2.5 mM MPP^+ and intracellular ATP levels were measured after various periods of time.

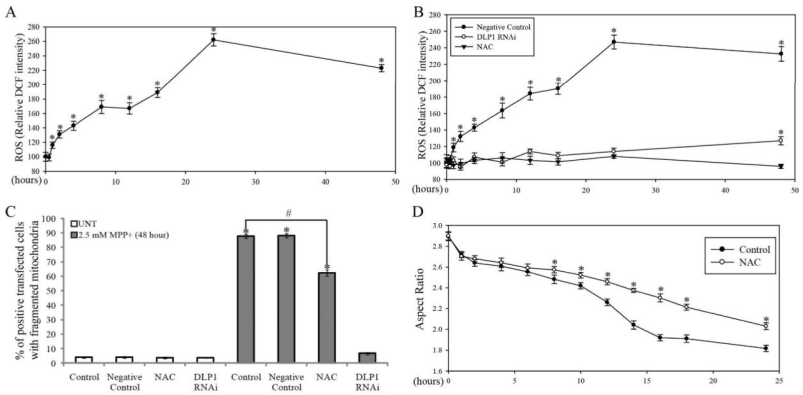

Figure 5. MPP^+-induced mitochondrial fragmentation and ROS production

SH-SY5Y cells seeded on 96 well plates were treated with 2.5 mM MPP^+ and ROS levels were measured after various periods of incubation time (A). (*p<0.05, when compared with the control cells without MPP^+ treatment; student-t-test.). (B) ROS levels in SH-SY5Y DLP1 RNAi cell lines or cell lines expressing RNAi negative-control vector treated with 2.5 mM MPP^+ for various periods of time. ROS level in SH-SY5Y cells co-incubated with 10 mM NAC and 2.5 mM MPP^+ was also measured. Experiments were repeated three times. (*p<0.05, when compared non-treated cells; student-t-test.). (C) Quantification of mitochondria morphology in control or DLP1 RNAi SH-SY5Y cells fixed after being treated with 2.5 mM MPP^+ for 48 h. The effect of NAC (10 mM) on MPP^+ induced-mitochondria fragmentation was also analyzed. (*p<0.05, when compared with the control cells without MPP^+ treatment; #p<0.05, when compared with control cells with MPP^+ treatment; student-t-test). (D) Quantification of aspect ratio as an index for mitochondrial morphology in live SH-SY5Y cells treated with 2.5 mM MPP^+ in the presence of 10 mM NAC. (*p<0.05, when compared with the control cells with MPP^+ treatment; student-t-test). At least 500 fixed cells or 20 live cells were analyzed in each experiment and experiments were repeated three times.

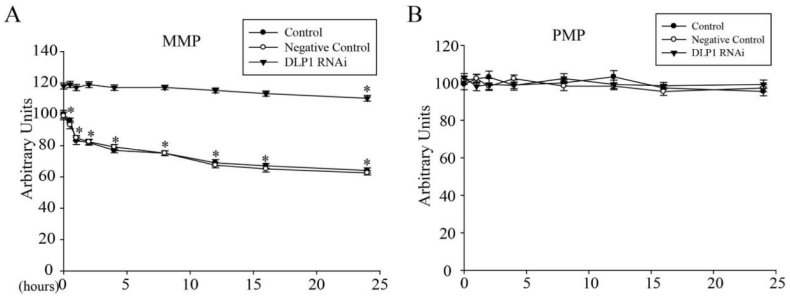

Figure 6. MPP^+-induced mitochondrial fragmentation and decreased mitochondrial membrane potential

SH-SY5Y cells seeded on 96 well plates were treated with 2.5 mM MPP^+ and the fluorescence intensities of TMRM for mitochondrial membrane potential (A) and DiBAC4(5) for plasma membrane potential (B) were measured after various incubation times. Experiments were repeated three times. (*p<0.05, when compared with the non-treated cells; student-t-test).

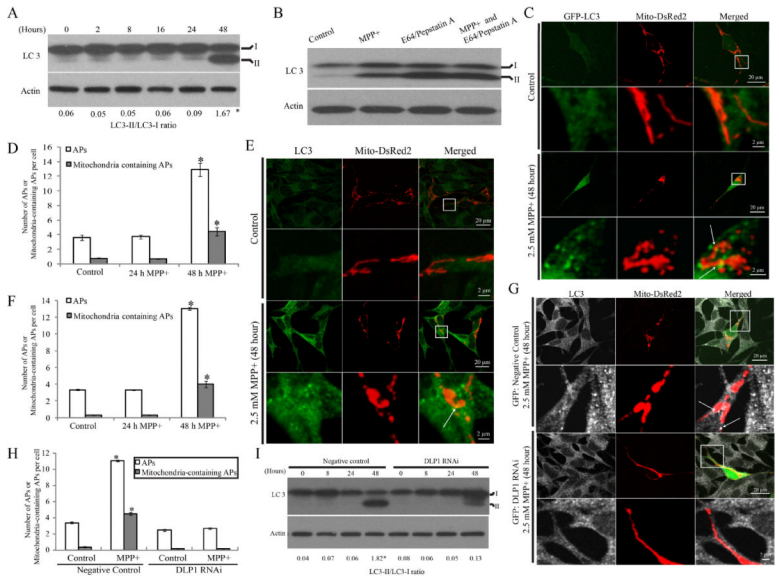

Figure 7. MPP$^+$-induced mitochondrial fragmentation was prerequisite for MPP$^+$-induced Autophagy/mitophagy

(A) Representative immunoblot of LC3 and quantification of LC3-II/LC3-I ratio in SH-SY5Y cells treated with 2.5 mM MPP$^+$ for various periods of time. (B) SH-SY5Y cells were treated with 2.5mM MPP$^+$ in the absence or presence of E64 (10μg/ml) and pepstatin A (10μg/ml) to inhibit lysosomal degradation. After 48 h, cell lysates were analyzed for LC3 by immunoblot. (C,D) To visualize autophagosome formation, SH-SY5Y cells were transiently co-transfected with GFP-LC3 and mito-DsRed2. Two days after transfection, cells were treated with 2.5 mM MPP$^+$ for 24 or 48 h. (C) and (D) are representative immunofluorescence pictures and quantification of autophagosome (AP) in cells transfected with GFP-LC3 and treated with 2.5 mM MPP$^+$ for 24 or 48 h. At least 50 cells were analyzed in each experiment. (E,F) Autophagosome formation was also assayed by direct immunostaining of LC3 in SH-SY5Y cells fixed after treatment of 2.5 mM MPP$^+$ for 24 or 48 h (E) and number of APs was quantified (F). At least 50 cells were analyzed in each experiment. (G,H) To study the effect of DLP1 reduction on MPP$^+$ induced autophagy/mitophagy, SH-SY5Y cells were co-transfected with empty/negative control vectors or DLP1 RNAi constructs and mito-DsRed2. Two days after transfection, cells were treated with MPP$^+$ for 48 h, fixed and stained by LC3 (G) and the number of APs was quantified (H). At least 50 cells were analyzed in each experiment. (I) Representative immunoblot and quantification analysis of LC3 in DLP1 RNAi SH-SY5Y cells after treatment of 2.5 mM MPP$^+$ for various periods of time. Equal protein amounts (10 μg) were loaded and actin was used as an internal loading control. All experiments were repeated three times. (*p<0.05, when compared with non-treated cells; student-t-test).

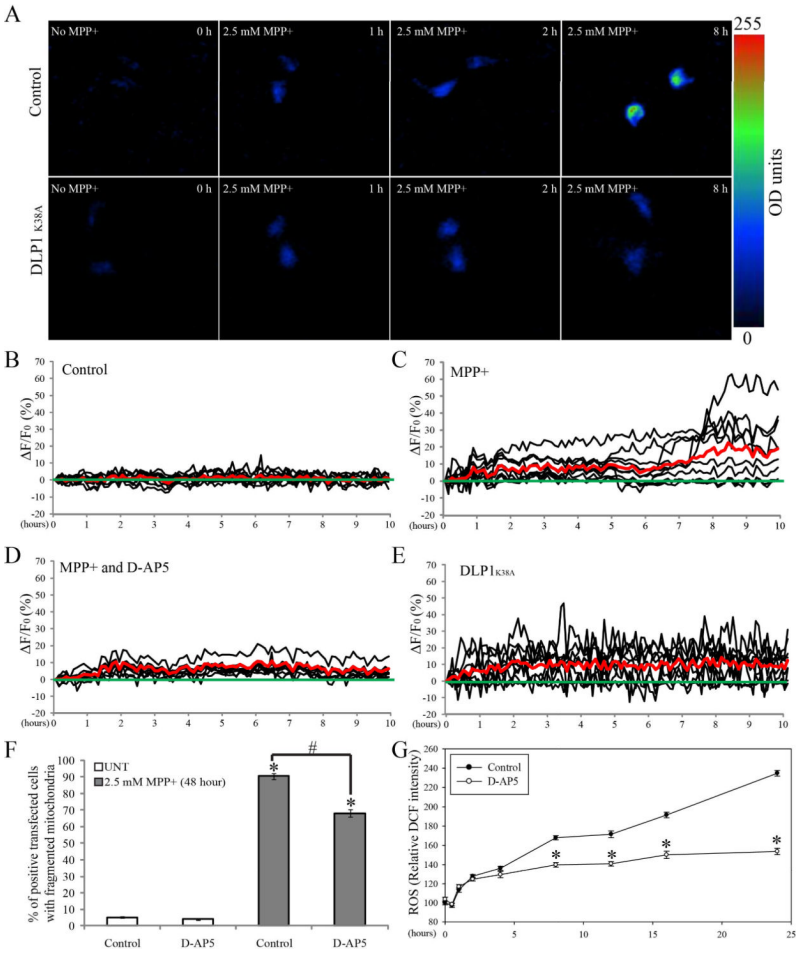

Figure 8. Activation of NMDA receptor activity contributes to MPP^+-induced mitochondrial fragmentation

SH-SY5Y cells seeded on dishes were transfected with Case12. Two days after transfection, cells were treated with 2.5 mM MPP^+ and imaged by fluorescence time-lapse microscopy. (A) Representative time lapse pictures of control or stable DLP1 K38A cells positively transfected with Case 12 in the presence of 2.5 mM MPP^+. (B–E) Record of intracellular Ca^{2+} levels ($[Ca^{2+}]_i$) from control cells, cells treated with 2.5 mM MPP^+, cells co-incubated with 2.5 mM MPP^+ and 50 μM D-AP5, or stable DLP1 K38A cells respectively. Case12 fluorescence values are presented as ΔF/F in % (ΔF/F = 100 · (F − F0)/F0. F is the fluorescence measured at different time points, while F0 is the baseline fluorescence). The oscillations of 10 representative cells are represented by black solid lines and the mean value of 50 cells are represented by red solid lines. (F) Quantification of mitochondria morphology in SH-SY5Y cells fixed after being treated with 2.5 mM MPP^+ and D-AP5 for 48 h. At least 500 cells were analyzed in each experiment. (*p<0.05, when compared with the control cells without MPP^+ treatment; #p<0.05, when compared with control cells with MPP^+ treatment; student-t-test). (G) Measurement of ROS level in SH-SY5Y cells co-incubated with 2.5 mM MPP^+ and 50 μM D-AP5 at different time. (*p<0.05, when compared with the control cells with MPP^+ treatment; student-t-test). All experiments were repeated three times.

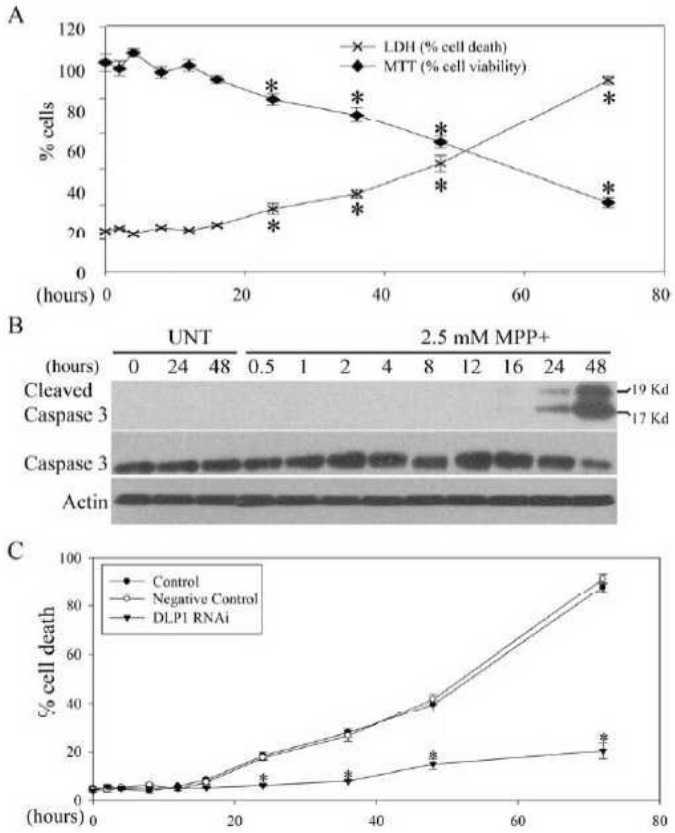

Figure 9. MPP$^+$-induced mitochondrial fragmentation preceded and was prerequisite for cell death

SH-SY5Y cells seeded on 96 well plates were treated with 2.5 mM MPP$^+$ and cell death/viability was determined by LDH release and MTT assays after various periods of incubation time (A). (*p<0.05, when compared with the control cells without MPP$^+$ treatment; student-t-test.) (B) Representative immunoblot pictures of cleaved caspase 3 and full length caspase 3 in SH-SY5Y cells treated with 2.5 mM MPP$^+$at different time points. Equal protein amounts (10 μg) were loaded and actin was used as an internal loading control. (C) Measurement of cell death by LDH assay in control, negative control and DLP1 RNAi SH-SY5Y cells treated with 2.5 mM MPP$^+$ at different time points. (*p<0.05, when compared with the control cells with MPP$^+$ treatment; student-t-test). All experiments were repeated three times.

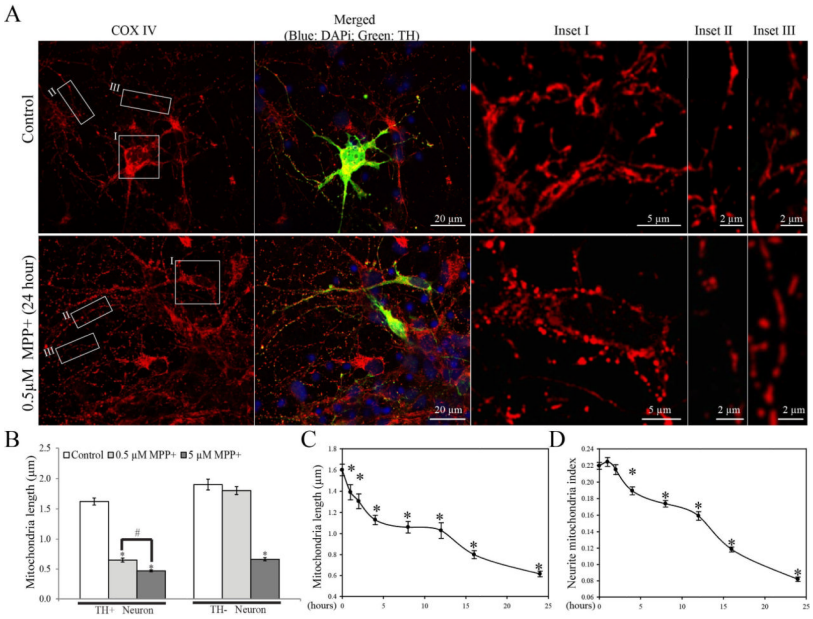

Figure 10. Effects of MPP^+ on mitochondrial morphology and distribution in rat E18 primary ventral midbrain TH-positive neurons

Midbrain neurons (DIV6) cultured on 8-well chamber slides coated with poly-D-lysine and laminin were treated with 0.5 μM MPP^+ for various periods of time, fixed and double immunolabeled for TH (Green) and COX-IV (Red). (A) Representative confocal microscopic pictures of primary midbrain neurons treated with or without 0.5 μM MPP^+ for 24 hours. Pictures of mitochondria in the soma (inset I) and neurite (inset II) of a TH-positive neuron and mitochondria in the neurite of a neighboring TH-negative neuron (inset III) were enlarged. Blue: DAPi. (B) Quantification of mitochondrial length in TH-positive and TH-negative neurons after 24 hr treatment of 0.5 or 5 μM MPP^+. (C–D) Quantification of mitochondrial length (B) and neurite mitochondria index (C) in the TH-positive neurons after treatment of 0.5 μM MPP^+ for various period of time. (B, C, D) Quantification was done on mitochondria in neuronal processes 400 μm in length beginning from the cell body. At least 20 TH-positive neurons were analyzed in three independent experiments (* comparing to non-treated controls, $p<0.05$, #$p<0.05$).